Summer 8-15-2019

Mechanosensitive epithelial cell scattering and migration on layered matrices

Christopher Michael Walter
Washington University in St. Louis

WASHINGTON UNIVERSITY IN ST. LOUIS

Division of Biomedical Engineering

Dissertation Examination Committee:
Amit Pathak, Chair
Elliot Elson
Robert Mecham
Gretchen Meyer
Lori Setton
Srikanth Singamaneni

Mechanosensitive Epithelial Cell Scattering and Migration on Layered Matrices

by

Christopher Walter

A dissertation presented to
The Graduate School
of Washington University in
partial fulfillment of the
requirements for the degree
of Doctor of Philosophy

August 2019
St. Louis, Missouri

Table of Contents

List of Figures

Acknowledgments

The work presented in Chapter 2 of this dissertation was previously published in part in the Royal Society of Chemistry Integrative Biology Journal, Issue 6, on May 16, 2018.

This work was supported in part by NIBIB Grant # T32 EB018266-02 awarded to Christopher Walter and NIGMS Grant # R35 GM128764 awarded to Amit Pathak.

I would like to thank all past and present members of Amit Pathak's laboratory for their assistance and support throughout this process. I would also like to thank my family and for their constant love and support. I would especially like to thank my parents who supported me and inspired me to pursue my dreams. I would finally like to thank my wife who supported me and suffered alongside me throughout the grueling process of obtaining my degree.

Christopher Walter

Washington University in St. Louis

August 2019

ABSTRACT OF THE DISSERTATION

Mechanosensitive Epithelial Cell Scattering and Migration on Layered Matrices

by

Christopher Walter

Doctor of Philosophy in Biomedical Engineering

Washington University in St. Louis, 2019

Professor Amit Pathak, Chair

Epithelial cells form multi-layered tissue scaffolding that makes up every organ in the body. Along with epithelial cells, the basement membrane (BM) and connective tissue are composed of various proteins that sculpt the organs and protect them from foreign macromolecules. Epithelial cells respond to various cues, both chemical and mechanical, from their surrounding matrices to aid in maintenance and repair of these layers through degradation and deposition of extracellular matrix (ECM) proteins. In cancer progression, epithelial cells lose their normal function of supporting tissue structure and instead adopt more aggressive behaviors through an epithelial-to-mesenchymal transition (EMT) of their cellular traits. In some cases, these cells may break away from the primary tumor and begin to develop a secondary tumor elsewhere, a process known as metastasis. In these processes, cells are constantly interacting with highly heterogeneous and layered matrices that can influence cell behavior. This dissertation investigates how mechanical properties of both intact and defective layered matrices influence epithelial cell response. Chapter 1 details an introduction to epithelium structure and health, as well as how the mechanical properties of the matrix supporting the epithelium structure regulate epithelial cell

behavior. Chapter 2 investigates the role of basement membrane (BM) integrity in maintaining epithelial monolayer health. A common outcome of EMT is degradation of surrounding ECM as cells become more mechanically active and migratory. Conversely, it is not known whether a break or defect in the BM could, in turn, induce EMT. We address this question in two parts. First, we layer BM-mimicking collagen-IV coatings onto tunable polyacrylamide (PA) hydrogels, induce a defect into the layered hydrogel, and then culture normal epithelial cell networks on the defect-laden substrates. Second, we layer the BM-like matrix atop a collagen matrix to investigate the impact of the BM defect on cell invasion. Our results show that defects in BM-mimicking substrates induce EMT in normal epithelial cells by promoting degradation of the BM itself, triggering mechanical activation of normal epithelial cells in 2D and further progressing EMT induction. We also demonstrate that BM defects can trigger epithelial cell invasion into the surrounding ECM through the same BM degradation mechanism. In chapter 3, we address the ability of normal and cancerous epithelial cells to sense distant matrix stiffness. Epithelial cells have been shown to be highly sensitive to substrate stiffness, particularly the stiffness of their immediate surroundings. However, epithelial cells reside in layered environments in which distinct layers stiffness and fiber structure can vary greatly. Yet, little is known about the ability for epithelial cells to sense these distant layers. Here, we investigate the extent to which distant matrix stiffness can affect cell migration by fabricating collagen-I matrices of varying thickness onto PA hydrogels of tunable stiffness. We have found that while normal epithelial cells are only able to sense the stiffness of their immediate surroundings, cancer cells show sensitivity to distant matrix stiffness through fibrous collagen matrices. Cancerous epithelial cells are able to sense distant matrix stiffness through greater actin fiber assembly, cell force generation, and by utilizing the fibrous intermediate collagen matrix to

deform the distant PA substrate. By inhibiting the force-generating cellular machinery or by crosslinking the collagen network, we eliminate the ability of cancer cells to sense distant matrix stiffness. Our findings show that cancer cells may be affected by more than just their immediate surroundings, and, in turn, may influence the behavior of distant epithelial cells.

Chapter 1: Introduction: Epithelial Health and Response to Layered Matrices

1.1 Epithelium

Organ structures throughout the body are comprised of a variety of proteins and cells, naturally arranged into layers. Starting with the outermost, the first layer consists of a sheet of epithelial cells. The shape of these can vary, however they generally form thin, tightly connected sheets that are important for maintaining organ health as a first layer of defense from external chemical signals and damage.[1,2] Epithelial cell sheets are held together through cell-cell contacts formed by gap, tight, and adherens junctions.[1] Cadherins, specifically E-cadherin, construct physical connection between the cells and thus enable communication of forces throughout the monolayer of cells.[1,3] This physical cell-cell communication is important for regulating the overall health of the epithelium. The cell-cell junctions are balanced by cell-matrix adhesions to the underlying thin sheet of matrix known as the basement membrane.[4]

The basement membrane is a thin sheet of various proteins, including multiple structural proteins, like collagens and fibrillin, and various anchoring proteins such as integrins and laminins.[5] Specifically, collagen type IV makes up the majority of the structural component to the basement membrane. Collagen-IV forms a thin (~50 nm thick) densely connected network within which the various anchoring proteins are "hooked."[5] This tight network of matrix proteins helps to maintain the health of the epithelial cells that reside on it, thereby also protecting the interior of the organ from inward transport of harmful elements, such as viruses and chemical factors.[6-8]

Attached to the basement membrane lies the connective tissue.[9-11] Whereas there are some specialty types of connective tissue, in general, the connective tissue is comprised of a structural interstitial matrix and sparse quantities of fibroblasts.[2] The interstitial matrix is composed of a fibrous network of collagens, mainly collagen type I, and elastin, a component that gives the tissue and organ its elasticity.[12] Individual collagen fibers form triple-helical fibrils, which then link with other fibrils to create an interconnected fibrous network of matrix.[13] The fibroblasts that reside within the matrix are responsible for maintaining this network through protein degradation, excretion, and network remodeling.[14,15] As mentioned previously, the connective tissue, as well as the other components of this layered nest are critically important to maintaining organ health and function and preventing serious diseases.

1.2 Epithelial Cell Sensing and Response

As mentioned previously, epithelial cells are anchored to the basement membrane through cell-matrix adhesions.[5] Through these adhesions, cells are able to deform the surrounding matrix and thus "sense" its various properties, both chemical and mechanical.[16-20] To sense their surrounding matrix, random polymerization of intracellular actin globules cause the cell membrane to bleb out and allow for connection of transmembrane proteins to anchoring matrix proteins. As internal polymerization of actin continues, cells begin to develop a front-rear polarity, which can be stochastic, or guided by external properties, such as matrix fibers or stiffness. As this planar cell polarity continues to develop, the actin cytoskeleton becomes reinforced, allowing for cells to generate greater forces, in turn able to greater sense their surrounding matrix. As cells sense matrix stiffness and topography, the internal protein production is simultaneously modified to alter cell behavior to appropriately accommodate its environment.

1.3 Epithelial Health

As extracellular properties change through varying stages of development or disease, broad changes in epithelial behavior can occur through the mechano-sensing ability of individual cells. Some of the important biological processes in which normal function of epithelial cells play critical roles include development, wound healing, and immune response.[21-28] Such malfunctions can also lead to dysfunction in epithelial layers, which can lead to many pathological abnormalities, including cancer and fibrosis.[29-35]

Epithelial cancers are some of the most aggressive due to their tendency to metastasize.[36-38] Metastasis is the process of cancer cells breaking away from the primary tumor, entering the blood stream, and then exiting the blood stream in a second location, beginning the development of a new tumor.[37,38] Although the circulatory system gives access to the entire body, some more common sites of secondary metastases include the lungs, bones, and liver.[39] As epithelial cells break away from the primary tumor site, they begin to adopt more aggressive phenotypes, suitable for degrading their surrounding matrix and migrating to surrounding blood vessels.[37] This process is known as the epithelial to mesenchymal transition (EMT). The unpredictability of epithelial malfunction and the resulting tumor invasion makes cancer difficult to treat.

1.4 Epithelial to Mesenchymal Transition

The EMT is a process through which epithelial cells lose their native, quiescent state and begin to express more aggressive phenotypes. Typically, this process is identified by changes in cell morphology, migration, and broad changes in their gene expression profile.[19,20,29,31,37,40-42] As cells begin to break away from their epithelial sheets, they become more polarized and develop a strong, coordinated actin cytoskeleton.[37] This cytoskeleton then becomes reinforced with vimentin, an intermediate filament, and microtubule assemblies.[38,43] This reinforced cytoskeleton

allows cells to generate greater forces, allowing for manipulation and restructuring of their surrounding ECM and faster migration.[38,43] Within the nucleus, various transcription factors become highly upregulated, promoting or modifying these listed behaviors as well as a litany of others, including proliferation, cell cycle maintenance, programmed cell death, and external signaling pathways.[19,29,37,38,44] It is through this process that epithelial cancers become unpredictable and both difficult to treat, as well as dangerous to health.

There are a number of environmental factors that can stimulate this behavior, such as chemical signaling[16-18], like that of signals from a neighboring tumor, and mechanical properties, such as stiffness, porosity, and geometry.[19,20] Understanding the effects of these properties on epithelium health and behavior are critical to the development of adequate, appropriate therapeutic strategies for treating aggressive epithelial cancers.

1.5 The Importance and Process of Cell Migration

An important aspect of tissue and organ development, wound healing, and cancer metastasis is cell migration. During tissue and organ development, cells must migrate to aid in forming the tissues themselves, while during wound healing, cell migration aids in closing the physical wound.[45,46] In cancer, a well-known dangerous aspect of tumor cells is the ability for cells to metastasize and migrate away from the primary tumor site to form secondary tumors elsewhere.

Cell migration is a multi-step process that involves the coordination of both intracellular and extracellular components. As described previously,[47] cells first probe their immediate ECM and create focal adhesions with local ECM proteins. Due to the distribution of ligands and small differences in the microenvironment, the distribution of cell adhesions will tend to accumulate in one general direction.[47] As cells continue to create focal adhesions, actin filaments polymerize within the cell, aligning the cell in the direction of the focal adhesions, causing it to become

polarized.[48,49] As actin polymerization increases, actomyosin contractility forces increase along the actin fibers. Whether it be by ligand density or differences in local ECM stiffness, the force generated by the cell tends toward one direction. Once the force generated by the cell is greater than the opposing adhesive forces, the cell migrates in the direction of the leading edge. Due to the nature of this phenomenon, modifying and patterning the ECM in numerous ways, both chemical and mechanical, can control cell migration.

1.6 Significance of Understanding Epithelial Cell Behavior in Layered Matrices

Previous studies have indicated that matrix stiffness is a potent regulator of a variety of cell behaviors in a variety of cell types. Mesenchymal stem cells have been shown to differentiate into neuronal cells on soft substrates, while on stiff substrates they differentiate into osteoblasts.[22] Fibroblasts and smooth muscle cells are also sensitive to substrate stiffness, showing increases to cell area and polarity, reduction in cell roundness, and faster migration on stiff substrates.[23,50-53] Much like these other cell types, epithelial cells have been shown to exhibit sensitivity to a variety of substrate properties, including changes to cell morphology, migration, and the process of EMT.[19,54,55]

As the matrix stiffness increases, so does the propensity for epithelial cells to undergo EMT, as seen by their increase in cell area, polarization, and migration speed.[19,54,55] These behaviors occur as a result of upregulation of pro-EMT genes, or genes that promote more aggressive, mesenchymal behaviors, such as SNAI1 and Zeb1.[29,56,57] When grown on substrates of varying stiffness, epithelial cells show a tendency to gravitate towards the stiffer substrate, both as single cells and whole cell collectives.[23,58] These behavioral changes all contribute to an overarching behavior similar to that of cancerous epithelial cells.

These previous studies have laid the groundwork of how epithelial behavior responds to changes in the stiffness of their immediate environment. However, as I previously stated, the native ECM is a highly layered matrix, comprised of a variety of proteins and cells, each having their own contribution to the equilibrium of epithelial structures. It is possible that distant matrix properties could affect epithelial cell behavior much like the immediate matrix properties. How cells are able to distinguish these layers is still relatively unknown. Previous work has begun to investigate the ability for cells to sense distant stiffness, but the results and studies themselves have been limited. For smooth muscle cells, cardiomyocytes, and epithelial cells, it has been shown that as substrate (soft polyacrylamide) thickness was increased, the distance from the underlying stiff glass increased and cell spreading decreased, similar to cells on soft substrates.[59-62] In this 'deep sensing' of distant matrix stiffness, the ability of cells to form robust adhesions and generate forces is found to be a critical component.[60]

A limitation to these studies is the choice of substrates used to represent the layers in the native ECM. The collagen structure found within the connective tissue is highly fibrous and viscoelastic, directly contrasting the linear elastic polyacrylamide matrix.[63-66] In order to better understand how layered matrices and distant matrix properties affect epithelial cell behavior, more accurate experimental platforms must be created to represent the *in vivo* nature in which epithelial cells reside. Understanding the effect of both distant and immediate ECM properties on cell behavior is key to developing a greater understanding of many biological processes, as well as developing adequate treatment therapies for pathologies arising from epithelial dysfunction.

Chapter 2: Physical defects in basement membrane-like collagen-IV matrices trigger mesenchymal transition in normal epithelial cells

2.1 Introduction

In pathogenesis of cancer and fibrosis, the epithelial integrity is compromised through an epithelial-mesenchymal transition (EMT) of cells.[67] Additionally, the basement membrane (BM) matrix is degraded as the disease conditions progress.[9] As a result of these cellular and extracellular malfunctions, the cells transformed by the EMT invade through the BM and into the surrounding stroma.[68] Despite the known importance of the integrity of epithelial junctions and BM composition in healthy tissues, a connection between their dysfunctional transformations remains unclear.

The BM matrix is a thin and dense sheet-like network of extracellular matrix (ECM) proteins, which is connected to the basolateral side of epithelial or endothelial cells throughout mammalian organs and tissues.[69] This membrane is essential for maintaining the health of the underlying tissue by providing structural support at the epithelium-stromal interface and serving as a barrier to foreign macromolecules.[6] Healthy BM structure plays an important role in preventing the invasion of cancer cells into the vasculature.[7] In breast cancer metastasis, basement membrane degradation is one of the key steps in the transformation of an *in situ* tumor into an invasive one.[70] Collagen type IV (col-IV) is the majority constituent in the BM composition, along with laminins, heparan sulfate proteoglycans, and nidogens.[7,8] The col-IV fibrils in the BM form a highly cross-linked network with occluded binding sites for other

proteins.[71,72]. This networked col-IV prevents BM degradation and invasion of attached epithelial cells into the stromal matrix.[7,9-11] However, as epithelial cells undergo EMT, they start to break cell-cell junctions, become fibroblastic, and attain motile characteristics, enabling them to deform and degrade their underlying BM; all of which are crucial early events in tumor invasion.[67] It is now known that matrix stiffness triggers EMT in epithelial cells through cellular mechanoactivation.[73-75] Furthermore, matrix topography, confinement and spatial patterning of ligands can induce EMT-like signatures in epithelial cell populations.[19,76,77] These matrix-dependent mechanosensitive modes of EMT are particularly relevant for fibrosis[78] and cancer,[75] where mechanical properties of the tissue microenvironment undergo dramatic changes during disease progression. Thus, it is possible that physical heterogeneities in the BM could break the symmetry in normal epithelial layers and trigger similar ECM-dependent pathogenic cellular transformations.

The EMT and associated stimulation of matrix metalloproteinases (MMPs) and cellular mechanoactivation have been shown to degrade the BM matrix in wound healing,[30] development,[42,79] and cancer progression.[80,81] Aside from pathological reasons and cellular transformations, the BM matrix can also sustain damage due to physical wounds, incisions, or surgeries. Although a homogeneous soft BM matrix is known to protect the epithelial state, it remains unknown whether mechanical heterogeneities and defects in the BM contribute to pathologically-relevant cellular transformations. In this study, we ask this converse question – can preexisting physical defects in healthy and soft BM-like matrix cause EMT and invasion in normal epithelial cells? If true, this finding will reveal that the heterogeneous transformation of the BM structure during disease progression is not merely a passive outcome but an active instigator of cellular EMT.

To address this question, we fabricated a soft polyacrylamide (PA) gel, one that protects against EMT, functionalized a layer of col-IV to mimic BM-like properties, and manually introduced a tear in the gel. Given that col-IV represents the majority structural component of the BM matrix and that physical properties of the BM are the focus of our study, we chose it as the primary ECM protein for our *in vitro* BM-mimicking scaffolds. We cultured MCF10A human mammary epithelial cells and found enhanced EMT markers around this physical matrix defect. We also measured how two different anomalies in the BM-like matrices – physical defects in soft matrix or homogeneous stiff matrix – cause EMT and cellular mechanoactivation. Through a new computational model that integrates cellular forces, cell-cell junctions, mechanoactivation and EMT in a multi-cell network, we simulated the spatiotemporal evolution of EMT progression and cellular mechanoactivation around the defect. Through a novel 3D scaffold combining both BM-like and stroma-like matrices, we showed that the defect-induced EMT not only persists in 3D, but also causes downward cell invasion. These findings demonstrate that the known degradation of BM caused by cellular EMT and invasion[68] might not be a one-way process. Instead, our results reveal a previously unidentified ability of normal epithelial cells to exploit the physical defects in the BM matrix to attain EMT and invasive phenotypes.

2.2 Materials and Methods

2.2.1 Fabrication of collagen IV-coated PA gels with defect

Glass coverslips were activated by plasma cleaning and Bind-Silane solution (94.7% ethanol, 5% acetic acid, and 0.3% Bind-Silane). After 10 minutes, the coverslips were washed in ethanol and air dried. Polyacrylamide gels were synthesized by free-radical polymerization according to protocols previously established.[55,63,82] Precursor solutions combining acrylamide,

bis-acrylamide, and ultrapure water were mixed at a ratio of 10%, 0.15%, and 89.85% respectively for ~50 kPa and 4%, 0.2%, 95.8% for ~0.5 kPa stiffness, as characterized before[82] and confirmed here (Fig. 2.1). A solution of 10% ammonium persulfate was added along with N,N,N',N'-tetramethylethylene diamine (TEMED) at 1:200 and 1:2000 v:v, respectively. Polyacrylamide solution was applied to the activated coverslips using a Sigmacote (MilliporeSigma, St. Louis, MO) treated microscope slide and allowed to polymerize for 30 minutes. Formed gels were functionalized with 0.5 mg/mL solution of sulfosuccinimidyl 6-(4'-azido-2'-nitrophenylamino) hexanoate (Sulfo-SANPAH) (Thermo Fisher Scientific) prepared in 50mM HEPES buffer (Santa Cruz Biotechnologies) and crosslinked to the PA surface upon activation with 365 nm UV for 10 minutes. Gels were then washed 3 times before applying a 0.5 mg/mL solution of type-IV collagen from human placenta (col-IV) (Millipore Sigma, St. Louis, MO). After col-IV application, coverslips were placed at 4^{o}C overnight (<12 hours), then washed. A scalpel was used to make an incision 1 cm in length immediately prior to cell addition. Cells were plated onto gels within 24 hours of col-IV deposition.

2.2.2 Cell culture

MCF-10A cells were cultured in DMEM/F12 supplemented with 5% horse serum, 0.2% Normocin, 20 ng/mL EGF, 0.5 mg/mL hydrocortisone, 100 ng/mL cholera toxin, and 10 μg/mL insulin, as previously established.[82-84] Media was changed every 3 days. For MMP9 inhibition experiments, cells were treated with the MMP9 Inhibitor (CAS 1177749-58-4; Calbiochem) at 5 nM concentration.

2.2.3 Immunofluorescence and image analysis

After 1, 3, or 6 days of culture, the cells were fixed with 4% Paraformaldehyde for 10 minutes, washed, and permeabilized using 0.1% solution of Triton X-100 for 15 minutes. Cells

were washed again and non-specific binding was blocked by 3% Bovine Serum Albumin (BSA) solution in PBS containing 0.1% Tween-20 for one hour. Primary antibody solutions were incubated overnight at 4^{o}C. Secondary antibody solutions were incubated for one hour at room temperature. Primary antibodies used were against col-IV (1:500; Abcam,), MMP9 (1:500; Invitrogen), E-Cadherin (1:200; Cell Signaling), pMLC (1:500; Invitrogen) and Vimentin (1:750; Pierce Biotech). Secondary antibodies used were goat anti-rabbit Alexa 647 (1:300; Life Technologies) and goat anti-mouse Alexa 488 (1:300; Life Technologies). F-actin was stained using rhodamine phalloidin (1:400; Life Technologies). Once stained, coverslips were mounted in Slowfade Diamond with DAPI (1:250; Life Technologies) onto microscope slides and sealed with a number 1.5 coverslip. Images were taken using an Olympus FV1200 scanning laser confocal microscope using an UAPON 40XW340 objective. Unless otherwise specified, all experiments were carried out with 3 experimental replicates and at least 6 technical replicates. Image analysis was performed using FIJI. E-cadherin membrane localization was calculated by dividing the E-cad expression on the cell membrane by the total E-cad expression to obtain a normalized ratio for each cell. Quantification of vimentin, pMLC, and col-IV was performed by measuring the pixel intensity per unit area in images with a cell monolayer present and only in areas in which cells were present (areas beyond the defect were not considered in the calculations). To quantify actin fiber formation, the average background intensity across all conditions was calculated and subtracted from each image, leaving behind only the high intensity actin stress fibers. Pixel intensity was then calculated from these images. To account for discrepancies in cell number and monolayer area, only data from full, unbroken areas of the monolayer were considered and all data were normalized by the area measured. Long-distance vimentin images were obtained by imaging gel constructs with complete monolayers that

extended >3 mm from the induced defect. Images were acquired in tiles using a laser-scanning confocal microscope (Ziess LSM 810; Carl Ziess MicroImaging; Germany) using a 40X objective and stitched together using ZEN2.1 software.

2.2.4 Fabrication of multi-layered 3D matrices and invasion analysis

To measure 3D cell invasion around the defect, a 3D ECM was fabricated by layering a coating of BM-mimicking col-IV on top of a matrix of stroma-mimicking Rat Tail Type I collagen (col-I; Santa Cruz Biotechnology). First, polyacrylamide gels were synthesized on coverslips and treated with Sulfo-SANPAH as with the aforementioned 2D substrates, after which 50 µL of col-I at a concentration of 0.5 mg/mL was applied and allowed to polymerize for 1 hour at 37^{o}C. After the col-I layer had polymerized, a 0.5 mg/mL concentration col-IV solution was applied and allowed to polymerize overnight at 4^{o}C. A crack was introduced after at least 12 h incubation. Cells were then seeded as a monolayer on the PA/col-I/col-IV layered scaffold and the cells were allowed to grow for 6 days. For immunofluorescence imaging, a similar procedure compared to the procedure used for the 2D gels was used here. A primary antibody against type-I collagen (Abcam) was used for staining the col-I matrix. Images were obtained using the Zeiss LSM 810 confocal microscope with 2 µm thick *z*-stacks. Invasion cell counts were obtained by counting the number of whole nuclei present within the 2 µm stack. Cell counts were also divided into 100 µm sections measured from the defect.

2.2.5 qPCR

Cells were grown on gels that contained 5 defects, spaced 3 mm apart, in order to maximize the number of cells exposed to the network break. These multiple cut gels were used for extracting mRNA for qPCR analyses. mRNA was extracted using Qiagen Quick RNA extraction kit (Qiagen) according to manufacturer's instruction. Primers for SNAI1, Zeb1,

PTEN, and RRNA18 (Qiagen) were used and experiments were performed using SYBR green (Qiagen). Results were normalized and evaluated by geometric mean outlined by Livak & Schmittgen.[85]

2.2.6 AFM

Atomic Force Microscopy (AFM) measurements of polyacrylamide gels were made using an MFP-3D-BIO atomic force microscope (Asylum Research, Santa Barbara, CA). Olympus TR400PB AFM probes with an Au/Cr coated silicon nitride cantilever and pyramidal tip were used, with spring constants ranging from 20-30 pN/nm as measured by thermal calibration (Asylum Research, Santa Barbara, CA). 50 μm x 50 μm force maps were taken at the location of the defect (<200 μm), away from the defect (>2 mm), and on control substrates, with 100 points per force map. Elastic moduli were extracted from force curves using a modified Hertz model, as described earlier.[86]

2.2.7 Statistical Analysis

Unless specified otherwise, results are reported as the mean $\pm$ Standard Error (SE). To identify the significant differences between two experimental conditions, an *F*-test was performed to determine whether equal variance could be assumed. Next, Student's *t*-test was used to determine significant differences between two groups. All statistical analyses were performed using the Data Analysis toolbox in Microsoft Excel. Differences were considered to be significant for $P<0.05$.

2.3 Physical defects in collagen-IV basement membrane induce EMT in 2D epithelium

2.3.1 Fabrication of layered BM-mimicking hydrogel substrates.

To culture cells on a BM-like substrate, we fabricated PA hydrogel substrates of defined stiffness, prescribed through ratios of monomer and crosslinker,[19,55,63] and of at least 100μm thickness on a glass coverslip (Fig. 2.1A). We picked a low PA stiffness of ~0.5 kPa, because it preserves the epithelial state of the cell monolayer in control matrix settings (homogeneous gel without defects). It is important to perform measurements of defect-induced EMT on soft substrates, because stiff ECMs are known to induced EMT through activation of the TGF-β signaling pathway, regardless of matrix topography or structure.[19,73,75,76,78] Next, we functionalized the PA gel surface and coated a layer of 0.5 mg/ml col-IV, which is a majority ECM protein in the BM matrix. Afterwards, we introduced a tear in the soft PA gel as described in Methods, resulting in an average defect width of ~40μm width (Figs. 2.1A,B,D).

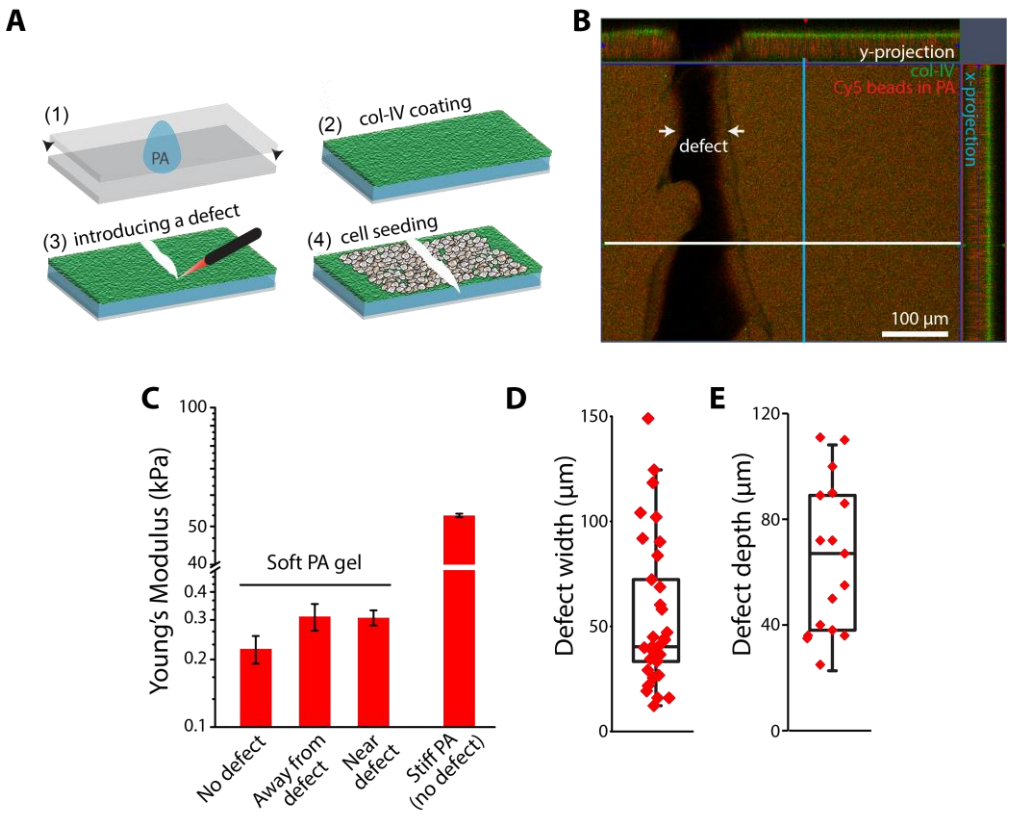

Figure 2.1. EMT induction around physical defects in soft BM-like col-IV matrix. (A) In four steps, soft PA gel is fabricated, col-IV layer is deposited, a defect is introduced in the form of a tear, and MCF10A cells are seeded. **(B)** Orthogonal projections of a representative immunofluorescent image with x- and y- profiles (blue and white lines, respectively) of the imposed defect in col-IV coated PA gels using col-IV antibody (Abcam) with Alexa Fluor 488 ELISA and 0.5 µm diameter fluorescent beads, respectively. This allowed for both defect width and depth measurements, averaging 54 and 65 µm, respectively. **(C)** Average Young's Modulus measured by AFM of soft PA gels prior to the introduction of defect (no defect), near the defect, and away from defect, as well as homogeneous stiff PA gels. **(D)** Average defect width measured via immunofluorescent images, as shown in (B). Box represents 25-75 percent of data. Whiskers represent outliers. Error bars = SEM. **(E)** Average defect depth measured via immunofluorescent images, as shown in (B). Box represents 25-75 percent of data. Whiskers represent outliers. Error bars = SEM.

Through Atomic Force Microscopy (AFM), as done previously,[55,86] we verified that the introduced physical defect in the PA gel does not cause significant change to its stiffness (Fig. 2.1C). Since only the top surface of the PA is functionalized and coated with protein, the inner

surfaces of the defect remain uncoated, prohibiting any attachment to the inside walls of the defect. By comparing col-IV images before and after introducing the defect (Fig. 2.2), we verified that cutting the gel does not create an aligned pattern of col-IV along the defect, which could have introduced an additional topographic cue. In rare cases, if some col-IV lands within

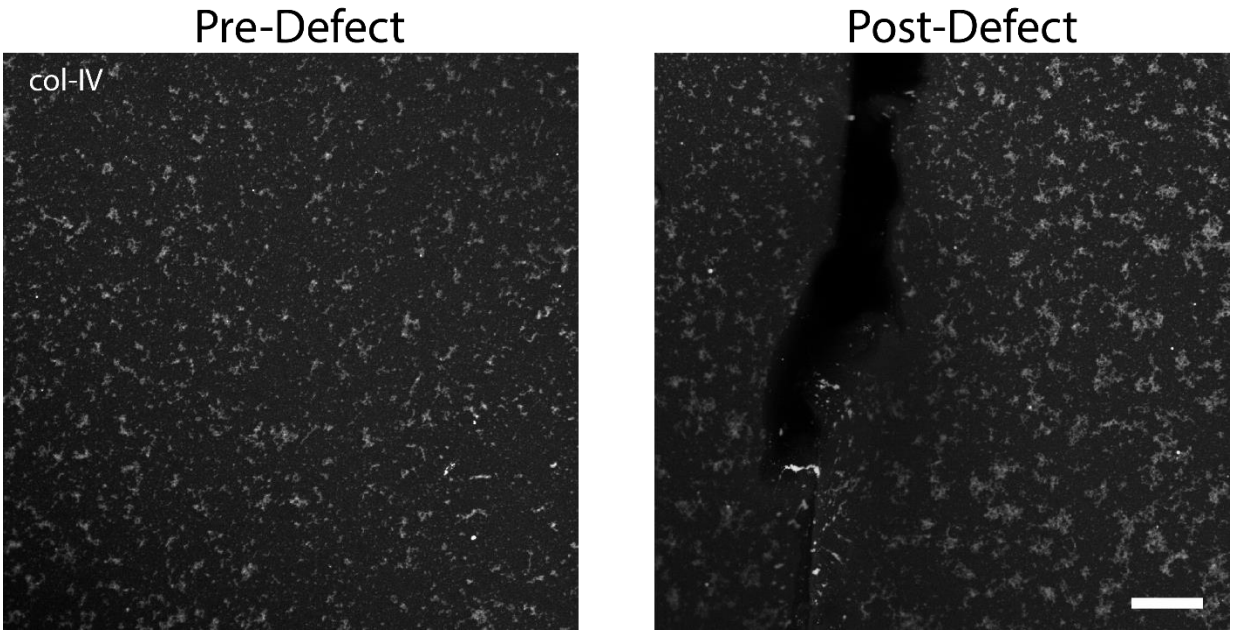

Figure 2.2. Creating defect does not result in loss of col-IV prior to cell seeding. Representative immunofluorescence images of col-IV before (left) and after (right) creating the defect. Scale bar=100 μm.

the valley of the defect, any cells within the defect (near the bottom surface) are unable to interact with the cell monolayer cultured on top of the PA gel (Fig. 2.3).

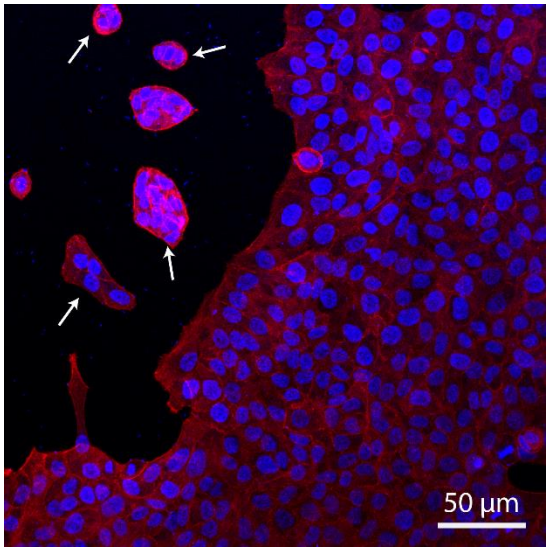

Figure 2.3. Cells that manage to seed at the bottom of the interior of the defect are unable to interact with cell monolayer. Representative immunofluorescence image of cell clusters at the bottom of the interior of the defect (white arrows) compared to the cell monolayer. Cells are stained for Actin (red) and DAPI (blue). Scale bar=50 μm.

2.3.2 Preexisting defect in collagen IV-coated soft matrix induces EMT in epithelial monolayer

On soft col-IV-coated PA gels, both with and without defect, we cultured MCF10A cell monolayers for 3 days. After fixing the samples, we stained and imaged for E-cadherin (an epithelial marker) and vimentin (a mesenchymal marker). For control measurements, we repeated experiments on homogeneous, i.e., without a defect, PA gels of the same stiffness. We observed a nearly 4-fold increase in vimentin expression due to the presence of the defect (Figs. 2.4A,B), a reduction in E-cad membrane localization by ~35% (Figs. 2.4A,C), and a rise in cell spreading and elongation (Figs. 2.4D,E), all of which are signatures of EMT. We also imaged for col-IV near the gel surface in each condition and found that the level of col-IV around the defect decreased by ~50% compared to the homogeneous substrates, which indicates col-IV degradation occurring concurrently with EMT induction (Figs. 2.4F, 2.5).

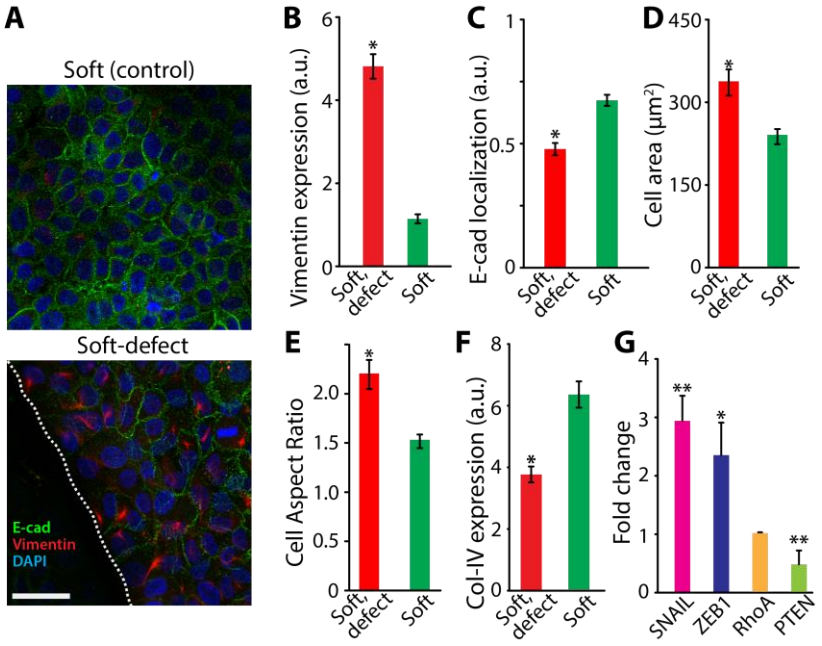

Figure 2.4. EMT induction around physical defects in soft BM-like col-IV matrix. (A) Representative immunofluorescence images of E-cad (green), vimentin (red), and DAPI (blue) in MCF10A monolayers on soft (0.5 kPA) PA gels with and without (homogeneous controls) defect. Scale bar=50 μm. **(B)** Average vimentin expression, **(C)** membrane localization of E-cad, **(D)** spreading area of individual cells within the monolayer, **(E)** cell aspect ratio, and **(F)** average col-IV expression. N>30. **(G)** qPCR measurements of SNAIL, ZEB1, RhoA, and PTEN levels relative to GAPDH controls, plotted as fold change (ΔΔct) compared to the levels on soft control matrices. Error bars = SEM. *p<0.01, and **p<0.001 compared to soft substrates.

To confirm EMT through molecular analyses, we extracted mRNA from MCF10A cells on gels with and without defects and performed qPCR. We chose primers for SNAIL, ZEB1, PTEN, and RhoA as a marker for cell mechanoactivation. We found that the levels of SNAIL (SNAI1) and ZEB1, both of which are hallmark transcriptional factors for EMT, increased over two-fold (Fig. 2.4G). We also found that PTEN level, which dephosphorylates PI3K[87,88] to maintain epithelial phenotype, was reduced by ~50%. Surprisingly, the RhoA activation remained undetectable and similar to the control soft gels, even as the EMT markers were enhanced after 3 days of culture on defective gels. These findings show that physical defects in

col-IV-coated soft matrices can induce EMT in normal epithelial cells within 3 days of culture without a prior RhoA-based cellular mechanoactivation.

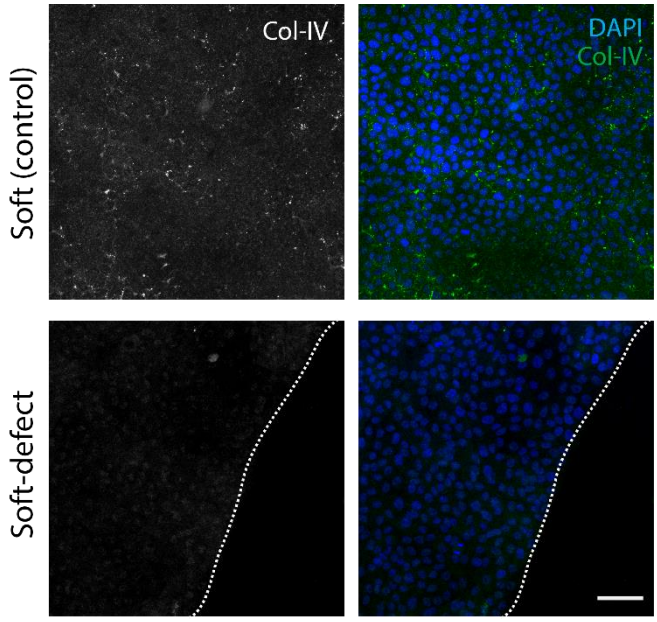

Figure 2.5. Presence of mechanical defect stimulates degradation of the underlying col-IV. Representative immunofluorescence images of col-IV and DAPI on soft control and soft-defect PA gels after 3 days of monolayer culture, corresponding to the data presented in Fig. 2.4F. Dashed line is used to emphasize edge of defect. Scale bar=50 μm.

2.3.3 Stress fiber formation on soft col-IV matrices rises after defect-induced EMT, but stiff matrices induce EMT and stress fibers more rapidly and concurrently.

To measure the chronological sequence of EMT and stress fiber formation, a signature of cellular mechanoactivation, we compared the expressions of aligned F-actin fibers, phosphorylated myosin light chain (pMLC), and vimentin after 1, 3, and 6 days of cell culture on the defective soft matrix (Fig. 2.6). Cells cultured for only 1 day on soft or defective soft matrices showed low vimentin expression (Fig. 2.6). After 3 days, however, vimentin expression on defective soft matrices increased by over 3-fold compared to day1 and by nearly 4-fold

compared to the homogeneous soft matrices, continuing to increase by another ~50% over 6 days (Fig. 2.6B). In contrast, for the soft-defect case, the expression of actin fibers remained low in the first 3 days and then rose by more than 5-fold over 6 days (Fig. 2.6A,C). Since stress fiber activity combines both actin and myosin expressions, we also measured pMLC expression (Figs.

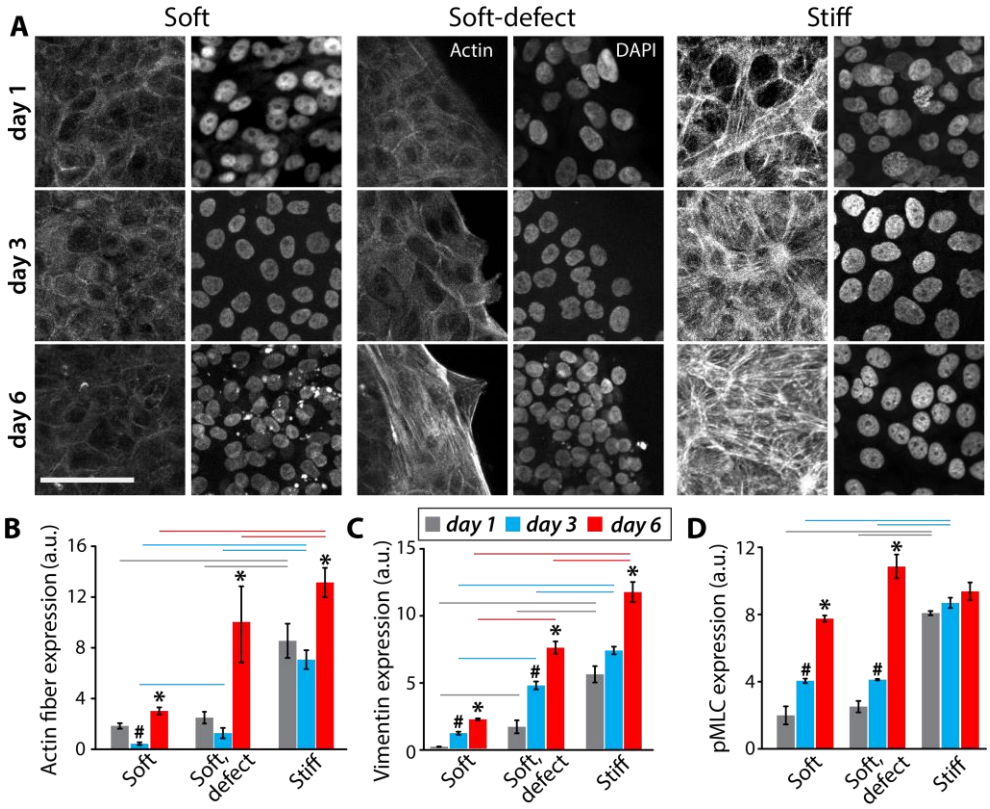

Figure 2.6. Defect-induced EMT precedes stress fiber formation, but stiffness-induced EMT and stress fibers evolve concurrently. (A) Representative immunofluorescence images of F-actin (red) and DAPI (blue) in MCF10A monolayers on soft, soft-defect, and stiff PA gels after 1, 3, or 6 days in culture. Scale bar=50 μm. Average expressions of **(B)** vimentin, **(C)** actin fibers, and **(D)** pMLC across the three ECM conditions after 1, 3, and 6 days. N>20. Error bars = SEM. *,# $p<0.01$ compared to soft control ECM. Horizontal lines above bars indicate $p<0.01$ between the indicated substrate conditions.

2.6D,), which followed trends similar to the actin fiber formation and vimentin expression.

Since the matrix-dependent EMT has conventionally been associated with matrix stiffening,[19,75,78] we compared EMT and stress fibers on col-IV-coated homogeneous (without defect) stiff matrices of ~50 kPa Young's Modulus (Fig. 2.1C). We found that vimentin

expression, pMLC, and actin fibers increased by the first day in culture and stayed high over 6 days of culture (Figs. 2.6A-D). These results indicate that soft col-IV matrix requires a defect to induce EMT, but sufficiently stiff matrix does not. To test whether slight stiffening of the matrix can trigger EMT in the absence of defect, we repeated these measurements after 3 days of culture on a col-IV coated PA gel of ~1.3 kPa stiffness, which is over three-times the stiffness of the control soft matrix, and found that vimentin expression and stress fiber formation remained at the

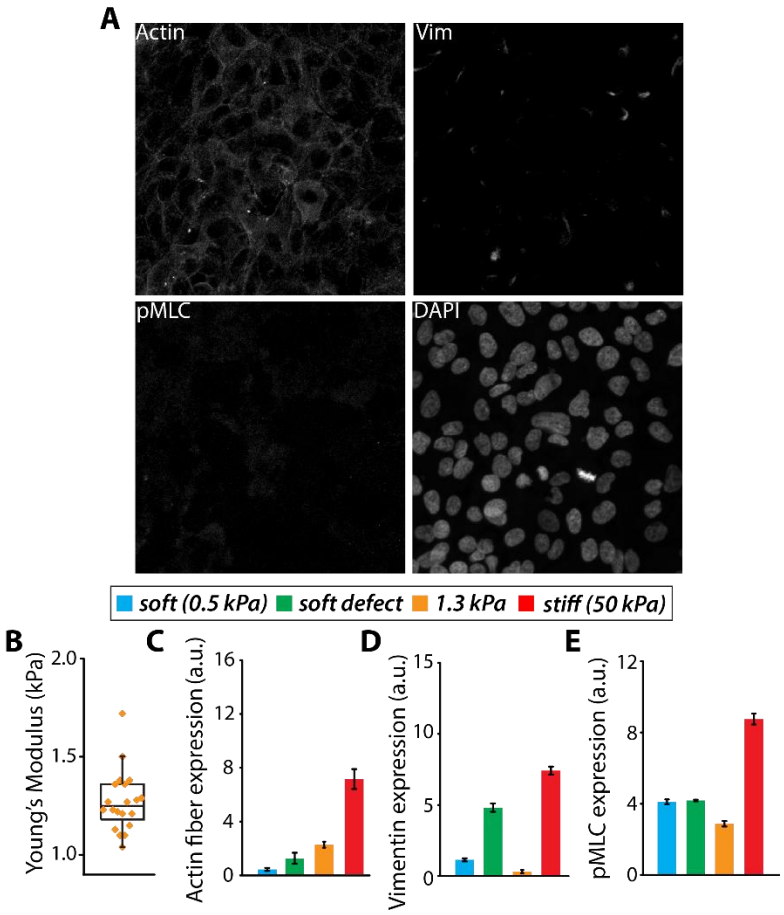

Figure 2.7. BM defect is necessary to induce EMT in MCF10a cells even on ~3x stiffer substrate. (A) Representative immunofluorescence images of actin, vimentin, pMLC, and DAPI in cells on BM substrates ~3x stiffer (1.3 kPa) than soft (0.5 kPa) substrates. Scale bar=50 μm. **(B)** Average Young's Modulus measured by AFM of 5% acrylamide, 0.2% bis-acrylamide PA. Average expressions of **(C)** actin fibers, **(D)** vimentin, and **(E)** pMLC across the four ECM conditions after 3 days. N>20. Error bars = SEM. Horizontal lines above bars indicate $p<0.01$ between indicated substrate conditions.

low levels observed for the control soft matrix (Fig. 2.7).

These temporal results highlight that the defective soft col-IV matrix first induces EMT within the first 3 days, which is followed by broad cellular mechanoactivation and further surge of EMT over 6 days. In contrast, on the stiff matrix, cellular mechanoactivation and EMT occur both rapidly and somewhat concurrently, with increased stress fiber formation and EMT markers within 1 day, followed by a continued rise over 6 days.

2.3.4 Inhibition of MMP9 disables col-IV degradation and defect-induced EMT.

Since EMT signatures rose without significant cellular mechanoactivation (stress fibers and RhoA activity) within 3 days for the soft-defect case, we sought to investigate other factors associated with the defective col-IV matrix. Earlier, we found a reduction in col-IV expression on the defective matrix compared to the homogeneous substrates (Figs. 2.4F, 2.5), which indicated cellular degradation of col-IV, enabled by the mechanically introduced defect. Given that MMP9 is known to play a crucial role in degradation of col-IV,[89] we repeated our measurements after treating the cells with a pharmacological inhibitor of MMP9. The efficacy of the inhibitor was confirmed using an MMP9 inhibitor assay kit (Abcam), as shown in Fig. 2.8.

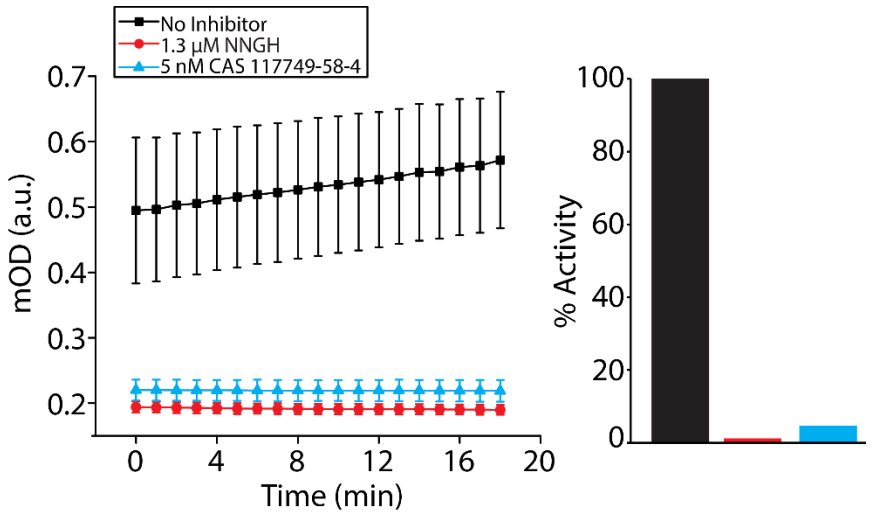

Figure 2.8. Validation of efficacy of used MMP9 inhibitor. Amount of MMP9 activity over time (left) and total activity (right) on samples with no inhibitor (black), supplied verification inhibitor (red) and experimental inhibitor used in this study (blue).

As expected, treatment with MMP9 inhibitor resulted in a loss of col-IV degradation on defective soft matrices (Figs. 2.9B, 2.10). The MMP9-inhibited cells showed dramatically reduced EMT markers, including vimentin expression and levels of SNAIL, ZEB1, and enhanced epithelial markers such as E-cad expression and PTEN levels compared to the untreated controls (Fig. 2.9). As a result, the MMP9-inhibited cells lacked expression of EMT markers in both soft-homogeneous and soft-defect matrix conditions. The RhoA activation continued to remain low in MMP9-inhibited cells (Fig. 2.9G). Notably, the MMP9-inhibted cells persisted to express robust EMT signatures on stiff matrices (Fig. 2.9, S8), which shows that the selected MMP9 inhibitor is not a generic blocker of EMT. In other words, the loss of the ability of cells to degrade col-IV disabled their sensitivity to the physical defect in the col-IV soft matrix and the cells only responded to the changes in matrix stiffness.

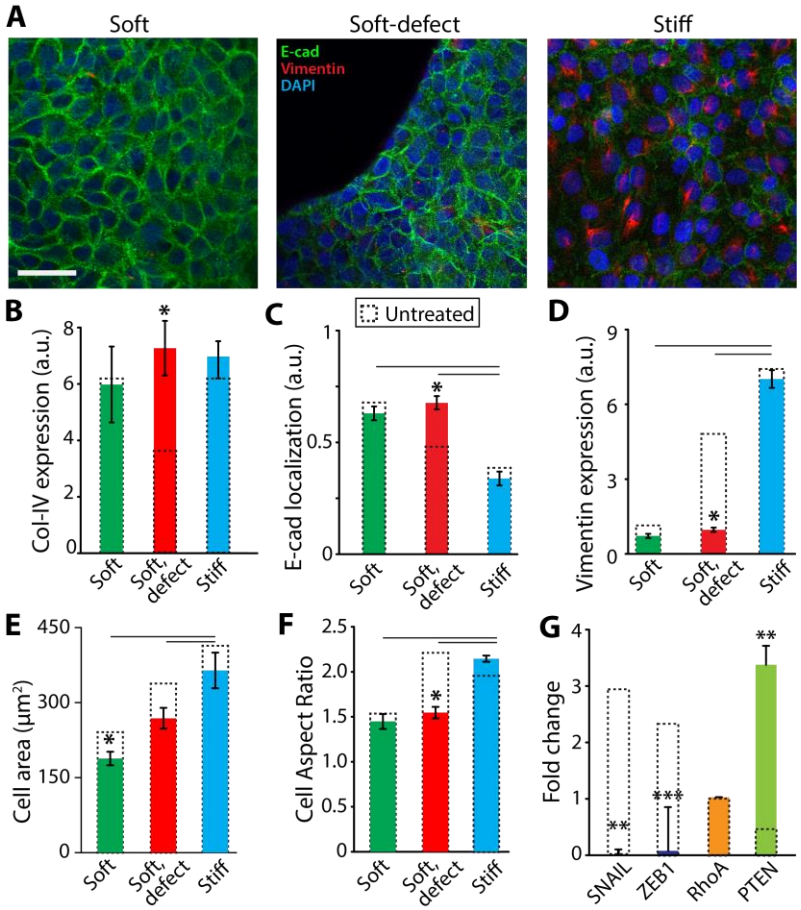

Figure 2.9. MMP9 inhibition blocks defect-induced EMT by disabling col-IV degradation. (A) Representative immunofluorescence images of E-cad, vimentin, and DAPI in MCF10A cell monolayer after treatment with MMP9 inhibitor on soft, soft-defect, and stiff PA gels. Scale bar=50 μm. Average expressions of **(B)** col-IV, **(C)** membrane-localized E-cad, **(D)** vimentin, and average **(E)** spreading area and **(F)** aspect ratio of MMP9-inhibted cells. N>30. *p<0.01 compared to untreated cells on the same substrate (dashed boxes). Horizontal lines above bars indicate p<0.01 between the indicated substrate conditions. **(G)** Fold change from qPCR measurements of SNAIL, ZEB1, RhoA, and PTEN levels relative to GAPDH control. Gray dashed boxes represent values for wildtype (without drug treatment) cells. Error bars = SEM. *p<0.01, **p<0.001, and ***p<0.001 compared to soft control ECMs.

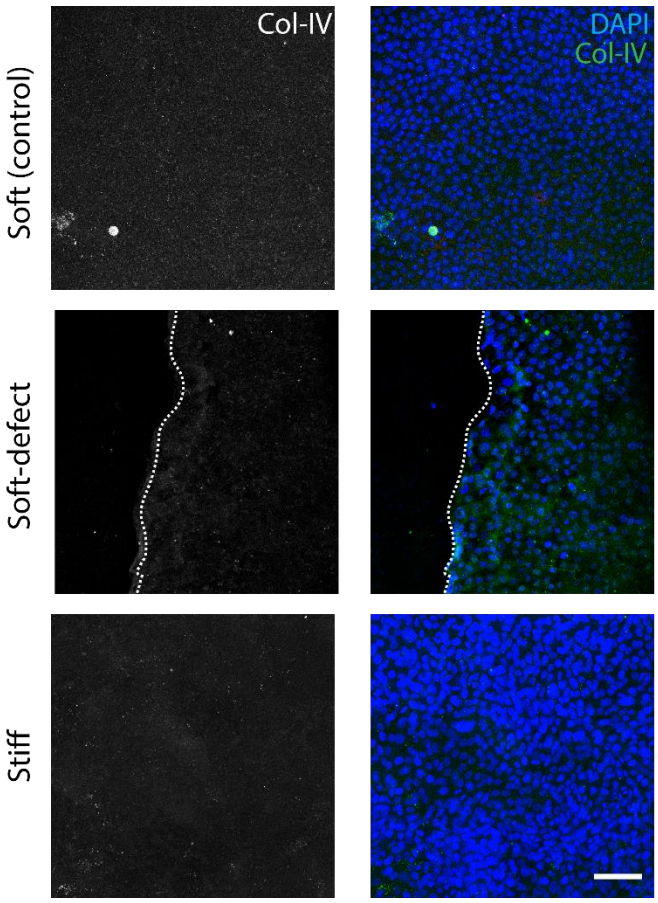

Figure 2.10. MMP9 inhibition stops col-IV degradation. Representative immunofluorescence images of col-IV and DAPI on soft control, soft-defect, and stiff PA gels after 3 days of monolayer culture of MMP9-inhibited cells show high levels of col-IV, corresponding to the data presented in Fig. 2.9B. Dashed line is used to emphasize edge of defect. Scale bar=50 μm.

2.4 Defect-induced EMT leads to 3D cellular invasion through collagen I matrices

An important biological consequence of EMT is the increased cellular invasion into the surrounding matrix, specifically stromal invasion in cancer cell metastasis.[67] To test whether the defect-induced EMT and cellular mechanoactivation causes these cells to invade in a 3D environment, we created a multi-layered gel substrate by first synthesizing a type-I collagen (col-I) gel on top of soft PA gels, then depositing a layer of col-IV on top of the col-I gel (Fig. 2.11A). It is important to use a soft PA gel as a foundation for this system, otherwise the cells might sense underlying stiff glass,[60,62] which is different from the conditions present *in vivo.* As before, we introduced a defect in the col-IV/col-I gel and seeded a cell monolayer on top.

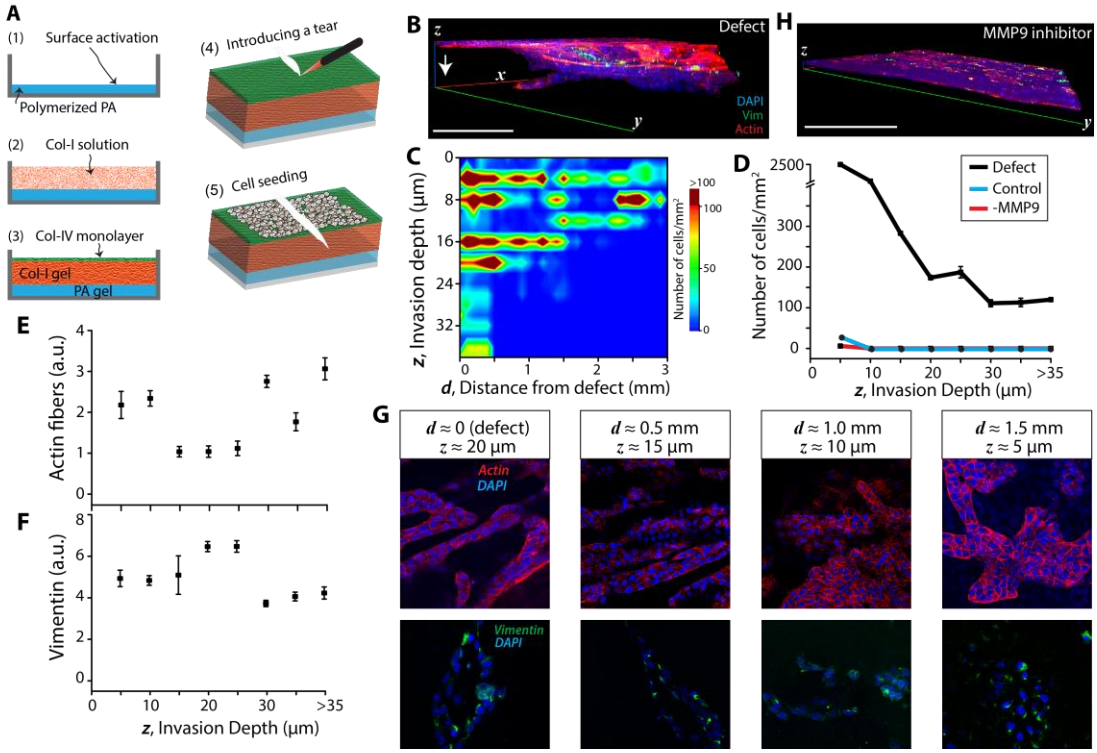

Figure 2.11. Defect-induced cellular EMT and mechanoactivation cause 3D invasion. **(A)** Schematic describing the fabrication of a multi-layered BM-stroma-mimicking scaffold with soft PA gels, 3D collagen I matrix, and a coating of col-IV. **(B)** Volumetric reconstruction of confocal immunofluorescence image z-stacks of actin, vimentin and DAPI showing the invasion of cells into this layered gel system with an introduced defect. Scale bar=50 μm. **(C)** Heatmap showing average number of cells at a given invasion depth, z, and distance from the defect, d. Quantification of **(D)** average number of invading cells per unit area, and **(E)** average vimentin expression and **(F)** average actin fibers versus invasion depth, normalized per unit area containing cells. Error bars = SEM. **(G)** Representative images showing the morphology and distribution of invading cell clusters through immunofluorescence imaging of actin, vimentin, and DAPI at various invasion depths (z) and distance from the defect (d). Scale bar = 50 μm. **(H)** Volumetric reconstruction confocal z-stacks showing negligible invasion of MMP9-inhibted cells around the defect. Scale bar=500 μm.

After 6 days of culture, we performed confocal microscopy to image for cells within the 3D col-I matrix, which showed extensive invasion of cells underneath the monolayer (Fig. 2.11B). We counted the number of cell nuclei within 5 μm thick confocal *z*-stacks and

discretized into 100 μm sections away from the defect. Across at least 7 different samples, we observed cell invasion over 30 μm deep into the col-I matrix around the defect (averaged within ~200 μm). These invasion depths reduced away from the defect (Fig. 2.11C); yet, we found ~10 μm deep invasion up to 2 mm distance away from the defect (Fig. 2.11B,C). Averaged over the area at any given distance from the defect, we found that over 2000 cells/mm^2 invaded at least 5 μm deep, while ~100 cells/mm^2 were able to reach invasion depths of more than 35 μm (Fig. 2.11D).

By imaging for actin and vimentin, we found that the invaded cells showed robust expressions of actin fibers and vimentin, indicating EMT induction and mechanoactivation, across varying depths of invasion and distance away from the defect (Figs. 2.11E-G). Cells that invaded more than 15 μm deep into the 3D col-I matrix showed tube-like formations (Fig. 2.11G; top row, left panels). In comparison, cells closer to the monolayer, i.e., smaller invasion depth, invaded in the form of larger sheets and clusters (Fig. 2.11G; top row, right panels).

Since earlier experiments in 2D showed that a defect is necessary for EMT stimulation on soft substrates and MMP9 inhibition disables EMT, we expected a similar outcome in these multi-layered gels. Indeed, in this 3D gel system, the systems without defects and those with MMP-inhibited cells showed negligible invasion (Figs. 2.11D,2.12). To verify that the col-I matrix remains intact around the defect, we stained and imaged for col-I and found robust col-I expression all around the invading cell population (Fig. 2.13).

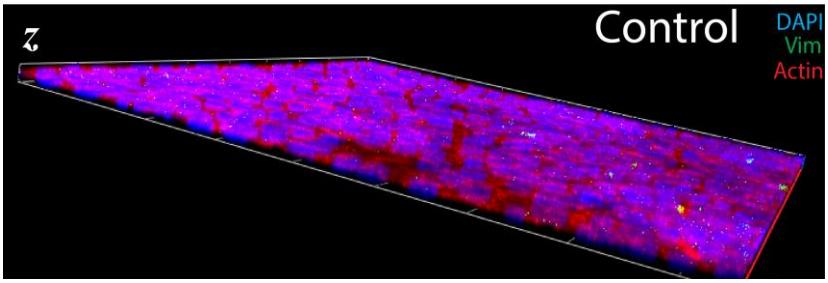

Figure 2.12. Cellular invasion and EMT do not occur without presence of defect. Volumetric reconstruction of confocal immunofluorescence image z-stacks of actin, vimentin and DAPI showing lack of invasion of cells on soft, control (no defect) 3D invasion substrates, corresponding to data shown in Figure 6. Scale bar=50 μm.

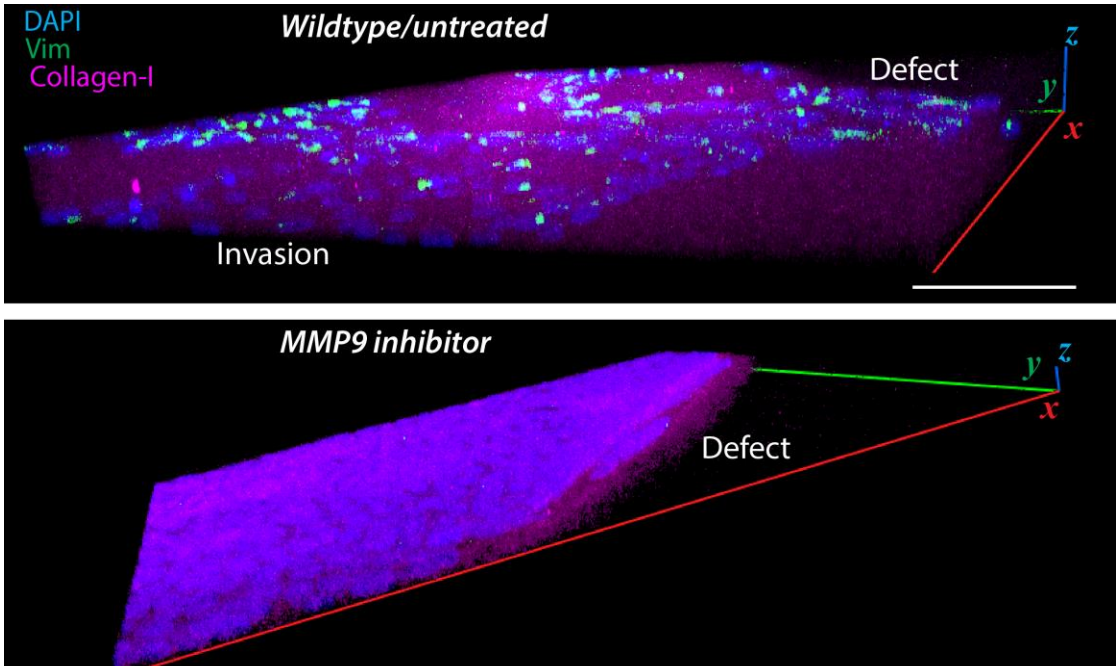

Figure 2.13. Collagen-I expression around the invading cells. Representative images of wildtype/untreated cells (top) and MMP9-inhibited (bottom) invading through the col-I 3D gels. After 6 days in culture, samples were fixed and stained for DAPI, vimentin, and type-I collagen. The presence of an intact col-I layer below the seeded monolayer and surrounding the invading cells indicates that cells are invading into the col-I layer, and not significantly degrading or sinking the monolayer as a whole. Cells treated with MMP9 inhibitor show no invasion and the col-I expression remains similar to the wildtype case. Scale bar = 50 μm.

2.5 Discussion and Conclusions

Our findings reveal that physical defects in the BM matrix can initiate disease-like cellular transformation in the form of EMT and invasion. Thus, the known BM degradation caused by the pathogenic transformation of cells through acquired EMT signatures might not be a one way process. Instead, physical composition of the BM matrix plays a more proactive role in triggering the disease-aiding EMT and motility in normal epithelial cells.

Through mechanotransductive signaling, stress fiber formation and morphological adaptation,[73-75,78,90] cellular EMT and invasion can respond to the stiffness and topography of their microenvironments,[19,75,76,83,90-94] which themselves undergo dramatic mechanical changes in cancer and fibrosis.[35,86,90,95,96] In particular, the basement membrane around tumors *in situ* undergoes degradation and becomes heterogeneous as cells exhibit mesenchymal signatures and tumor invasiveness increases.[81,97,98] Here, we have attempted to deconstruct this intricate coupling between EMT and BM heterogeneities in pathogenesis. We show that a preexisting defect in a BM-like soft matrix with a col-IV layer causes broad mesenchymal signatures in a sheet of normal MCF10A cells (Fig. 2.4). Given that edges in the matrix introduced due to microfabricated confinement[19] or micropatterned ligand patches[77] are known to induce EMT, we expected that the loss of cell-cell cohesion near the open boundary created by the defect would enhance cellular mechanoactivation, which in turn would lead to cell-cell dissociation and EMT. Although we did find enhanced EMT signatures around the BM matrix defect, surprisingly the RhoA activation and stress fiber formation remained low after 3 days of culture (Fig. 2.6). We also found the defect did not create an artificial space that cells could exploit for increased proliferation (Fig. 2.14). Thus, unlike the earlier cases of topographic confinement or ligand patterning,[19,77] the physical boundary created by the defect was not enough to increase cellular

mechanoactivation. Instead, the EMT was triggered by the degraded col-IV, which in turn enhanced cellular mechanoactivation. In retrospect, given that these experiments were conducted on a soft matrix, it is not surprising that the cells maintain low mechanoactivation and stress fiber formation regardless of a physical defect until EMT induction.

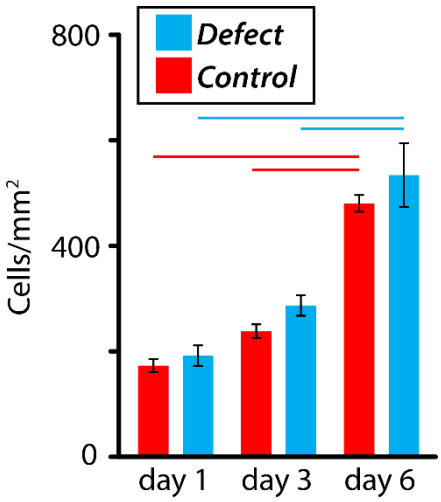

Figure 2.14. Cell proliferation increases over time, not spatially on soft-defect substrates. Average cells/mm^2 after 1, 3, and 6 days in culture on soft defect substrates. N>15. Horizontal lines above bars indicate p<0.01 between the indicated substrate conditions.

In another mode of matrix-regulated EMT, epithelial cells cultured on stiff matrix quickly undergo cellular mechanoactivation, marked by higher stress fiber formation and morphological elongation, developing somewhat concurrently with the EMT, as shown earlier [19,73-76,78] and reproduced here on a collagen IV-laden matrix (Fig. 2.6). In the case of defective BM matrix, stress fiber formation increases after the EMT induction over 6 days of culture. Thus, since the BM discontinuities led to cellular EMT even on a soft matrix and without stress fiber formation in the first 3 days (Figs. 2.4, 2.6), we concluded the main cause of BM defect-induced EMT is not cellular mechanoactivation. We observed that col-IV expression near the defect was lower than the control conditions, which indicated that the degraded col-IV fibrils around the defect

might directly initiate an EMT response. Consistent with this hypothesis, it has been previously shown that external introduction of col-IV fibrils into the culture media can induce EMT-like signatures in mammary epithelial cells.[99] Indeed, when the col-IV degradation was disabled through MMP9 inhibition, the EMT signatures around the matrix defect vanished. Notably, since the EMT on the stiff matrix persists even after MMP9 inhibition, it can be assumed that the used pharmacological inhibitor is not a universal EMT blocker.

Our results point to the following framework for BM defect-induced EMT – a tear in the col-IV network allows the cellular MMP9 to access col-IV binding sites and stimulate degradation; the degraded col-IV fibrils initiate EMT signaling within 3 days; the EMT induction propagates through the epithelial layer in a spatiotemporal manner; the defect-induced EMT and ECM stiffness can both independently enhance cellular mechanoactivation; the EMT-induced cellular mechanoactivation could provide a positive feedback for EMT.

In physiological settings, cellular EMT and mechanoactivation leads to cell migration and invasion through the surrounding tissue environments. We have shown that the EMT-based cellular transformation due to BM matrix defect triggers wide-ranging changes in the cells, including activated actin-myosin force machinery. On a defective collagen IV-laden 3D collagen I matrix, we found that the defect-induced EMT enabled the MCF10A cells to undergo EMT and invade through the collagen I matrix. Thus, physical defects in a BM-like matrix do not merely induce transient or benign forms of EMT and mechanoactivation signatures. Instead, these defect-induced cellular changes have real consequences for *in vivo* situations of BM degradation and stromal invasion, as clear from the measured distant 3D cellular invasion within 6 days of culture (Fig. 2.11). After MMP9 inhibition, both the EMT induction and cellular invasion completely stopped. In organ level experiments, overexpression of MMPs, through macrophages

and fibroblasts, has been shown to induce EMT.[100-102] In a new advance, we have discovered that normal epithelial cells can exploit preexisting defects in a soft BM matrix to degrade col-IV through MMP9 and attain disease-progressing phenotypes of EMT and 3D invasion. It is already known that MMP9 activity in immune and cancer cells potentiates lung metastasis,[103] promotes tumor vascularization,[104] and predicts breast cancer brain metastasis.[105] Additionally, upregulated MMP1 and MMP2 are known to degrade collagen-rich environments,[9,106] including the basement membrane,[107] and accelerate tumor invasion. Our findings provide further indication that MMP9 activity in particular may play a broad role in BM matrix degradation, which would further promote tumor cell invasion and stromal matrix remodeling through MMP1/2 activity.

Given that the BM microenvironment is composed of many proteins, including laminin,[7,8] the future *in vitro* BM models should go beyond the col-IV coating for improved *in vivo* impact of our findings of BM defect-induced cellular response. Rise in ligand density has been shown to diminish EMT even on stiff substrate through upregulation of integrin β4 and Rac1 activity.[108] Thus, it is possible that additional BM proteins might enhance cell-BM adhesions and reduce the defect-induced EMT invasion. Since laminin in particular has also been shown to play a critical role in breast cancer metastasis,[108,109] its presence in the BM matrix might provide better insights into cell invasion around defective BM matrix. With progressively increasing complexity, the BM-mimicking *in vitro* models are likely to provide a more accurate understanding of broad cellular response to mechanical defects and heterogeneities in the BM matrix.

.

Chapter 3: Epithelial cells sense distant stiffness through ECM deformation and realignment

3.1 Introduction

As cells interact with their extracellular environment, they sense and distinguish many different properties that influence and control their behavior. The mechanobiology field has robustly studied and shown how various cell types respond to the mechanical stiffness of their environment. Mesenchymal stem cells have been shown to alter their differentiation in response to substrate stiffness, becoming neuronal cells on soft substrates and osteoblasts on stiff.[22] Fibroblasts and epithelial cells have been shown to migrate faster on stiff substrates and their morphologies reflect these changes as they become more polarized and their spread areas increase.[19,26,54,55,110-113] In 3D, cells respond to more than just stiffness of their physical extracellular microenvironment. The fibrous architecture of 3D collagen hydrogels has been shown to guide cell migration through fiber bundling and realignment.[114-117] In 3D fibrous matrices, cells are known to sense and respond to the architecture of the fibers themselves, including the size of the fibers and the degree of crosslinking, both of which can be tuned *in vitro*.[118-121] All of these studies have shown how cells can sense the properties of their immediate matrix, yet, cells natively reside within a complex, layered matrix of variegated stiffnesses.[2] Furthermore, pathologies such as cancer dynamically alter matrix mechanics, which further adds to the complexity of the layered cellular microenvironment.

In tumorous environments *in vivo*, the stiffness of the ECM can vary across the scale of just a few cells. In invasive carcinomas, stiffness maps of mammary ductal tissues have shown highly heterogeneous stiffness, with changes of nearly 10 kPa over the range of just 5 μm.[122] Outside of cancer, ECM stiffness also greatly changes during wound healing and with the onset of fibrosis.[123-125] While we know that the cells that are in direct contact with these highly fibrotic, stiff environments are drastically affected, it is unknown if and to what extent cells away from these regions are affected.

It has been shown that cells are able to generate deformations through large distances in fibrous matrices. Fibroblasts and epithelial cells have been shown to deform and remodel their surrounding ECM.[126-128] In some cases, the effects of in-plane deformations can be seen up to 100 μm away.[129] With this in mind, and the heterogeneous nature of the tumor microenvironment, it is highly possible that the effects of regions of increased stiffness could stretch well beyond their immediate surroundings, possibly hundreds of microns away. This could have major implications in disease progression, where an increase in stiffness in one region could affect cell behavior in a distant region, causing matrix remodeling and stiffening, thereby extending the effect of the primary region. This further complicates the study and treatment of epithelial pathologies, such as cancer development and progression.

In breast tissue, cellular abnormalities can develop within the milk duct.[130] While they can start off as non-invasive, benign tumors, as the abnormality grows and restructures its microenvironment through matrix deposition and alignment, the tumor can quickly become invasive and malignant.[131] As this process occurs, we ask the question: can neighboring, yet distant, normal ductal cells sense this change and, in turn, become cancerous themselves? Also, can the cells within a developing ductal tumor, whether it be benign or malignant, sense the

stiffness of distant tumors, further exacerbating their invasive behaviors and remodeling of their local environment?

In this study, we present a novel multi-layered matrix scaffold and analyze single cell migration to tackle these questions. We layer a fibrous collagen gel of varying thickness on top of a polyacrylamide gel, whose stiffness we can tune, and then culture one normal (MCF10a) and one cancerous (MDA-MB-231) cell line on top in separate experiments. According to our measurements, while normal epithelial cells are unable to sense distant stiffness, cancerous epithelial cells are able to sense and adapt their behavior to distant substrate stiffness up to nearly 20 μm away. They are able to accomplish this through coordinated actin fiber accumulation and alignment, allowing them to generate an adequate amount of deformation in the intermediate collagen network to deform and sense the underlying, "distant" PA substrate.

3.2 Materials and Methods

3.2.1 Layered collagen-polyacrylamide gel fabrication

Polyacrylamide gels were made by mixing acrylamide and bis-acrylamide with ultra-pure water in the following acrylamide:bis-acrylamide (A:B) percentages of 4%:0.2% for 0.5 kPa PA and 15%:1.2% for 109 kPa PA. Stiffnesses were confirmed using AFM. After removing the air from the precursor solutions, ammonium persulfate (APS) and N-N'-N-N'-tetramethyl ethylenediamine (TEMED) were added to the mixture and PA gels were allowed to fully polymerize for 30 minutes. Gels were washed and stored in Dulbecco's Phosphate Buffered Saline (DPBS) (Fisher Scientific) at 4 C until layering of collagen was performed. Before addition of collagen, PA gels were sterilized using ultraviolet light for at least 30 minutes. After sterilization, gels were then treated with 0.5 mg/ml Sulfo-SANPAH solution (Thermo Fisher) to activate the surface of gels to allow for collagen attachment. Rat-tail collagen I (Advanced

Biomatrix) solution was prepared at a concentration of 1.3 mg/ml and adjusted to a pH ~8 using sterile NaOH. This collagen solution was then added in specified volumes on top of the activated PA gels and then allowed to polymerize in an incubator at 37 C and 5% CO_2. Collagen thickness was verified by adding fluorescent beads and measuring thickness using a Zeiss AxioObserver inverted microscope and quantified in Figure 1B. Cells were seeded immediately following collagen polymerization. For glutaraldehyde treated gels, after initial polymerization, layered substrates were incubated with 0.05% glutaraldehyde at 37 C for 30 min. Following treatment, gels were washed with DPBS and prepared for cell seeding.

3.2.2 Cell culture and tracking

MCF-10A epithelial breast tissue cells were cultured in tissue culture flasks as previously described [19] with DMEM/F12 (Invitrogen) supplemented with 5% (v/v) horse serum (Invitrogen), 20 ng/mL epidermal growth factor (EGF, Miltenyi Biotec Inc), 0.5mg/mL hydrocortisone (Sigma-Aldrich), 100ng/mL cholera toxin (Sigma-Aldrich), 10 ug/mL insulin (Sigma-Aldrich), and 0.1% (v/v) Normocin antibacterial, antifungal, and antimycoplasma cell media supplement (Invivogen). MDA-MB-231 epithelial breast adenocarcinoma cells were cultured with DMEM (Invitrogen) supplemented with 10% (v/v) fetal bovine serum (FBS) and 0.1% (v/v) Normocin. For cell migration studies, cells were seeded on top for 18 hours before being transferred to a Zeiss AxioObserver (Carl Zeiss Microscopy) inverted microscope with an incubation chamber kept at 37 C and 5% CO_2. For studies involving ROCK inhibition, cells were allowed to attach for 12 hours, after which culture media was replaced with media containing 10 μM Y27632 ROCK Inhibitor (EMD millipore). Cells were tracked at least 12 hours following initial seeding time. ImageJ (NIH) and the Manual Tracking plugin (NIH) were

used to quantify and sort cell tracks. Single cells were selected and tracked for a minimum of 4 hours. Tracks were then imported to MATLAB and analyzed using a custom script.

3.2.3 Immunofluorescence and confocal microscopy

After 2 days in culture, cells were fixed with 4% paraformaldehyde (Electron Microscopy Sciences). Cell staining was performed by permeabilization of cell membrane with 0.5% Triton-X 100 (Sigma-Aldrich) and blocking with 1% bovine albumin serum (BSA) (EMD millipore). After thoroughly rinsing the substrates with DPBS, cells were stained with 10mg/mL DAPI (Santa Cruz) and rhodamine phalloidin (Life Technologies) both at ratios of 1:500 (v/v) in staining buffer (0.5% BSA in DI water) for 30 min at RT. Confocal images were taken using a Zeiss LSM 880 laser-scanning confocal microscope (Carl Zeiss Microscopy). Images were analyzed using ImageJ (NIH).

3.2.4 Collagen deformation quantification and analysis

In order to track deformation in and through the collagen gel, 0.2 μm diameter fluorescent carboxylated polystyrene beads (Thermo-Fisher) were mixed into collagen solution at a 0.5% (v/v) dilution. 1 μm diameter fluorescent carboxylated polystyrene beads were also mixed into PA gels prior to polymerization in order to track deformation in PA as well. After cell seeding, collagen deformation was tracked on the Zeiss AxioObserver epifluorescent microscope. Deformations throughout the collagen gel were recorded in Z-stacks with 5 μm step sizes in order to visualize the entire gel. Bead movements were analyzed using the PIV software plug-in for MATLAB.[132,133]

3.2.5 Statistical Analysis

Unless stated otherwise, reported values are the mean $\pm$ standard error of the mean (SEM). To identify significant differences between any of the ECM conditions and drug treatments, ANOVA analysis was performed using Origin. Differences were taken to be significant for $p < 0.01$.

3.3 Results

3.3.1 Cancer cells sense distant matrix stiffness through a layer of collagen matrix, but normal cells do not.

To investigate whether epithelial cells sense distant stiffness, we fabricated a layered hydrogel system, consisting of a PA gel as the distant matrix and a collagen gel to simulate the immediate ECM. The PA gels were fabricated at 2 different stiffnesses: 0.5 kPa (soft) and 110 kPa (stiff) (Fig. 3.1C). Collagen was layered on top in three thicknesses: a monolayer "coating", a 10 μm "thin" gel, and a 50 μm "thick" gel (Figs. 3.1A,B). These stiffness and thickness variations lead to 6 different matrix scaffolds, which we will denote as: "soft-coated", "soft-thin", "soft-thick", "stiff-coated", "stiff-thin", and "stiff-thick". After fabrication, cells were seeded on top of the layered gels. To understand the ability of epithelial cells to sense distant stiffness, we tracked cell migration over two days in culture.

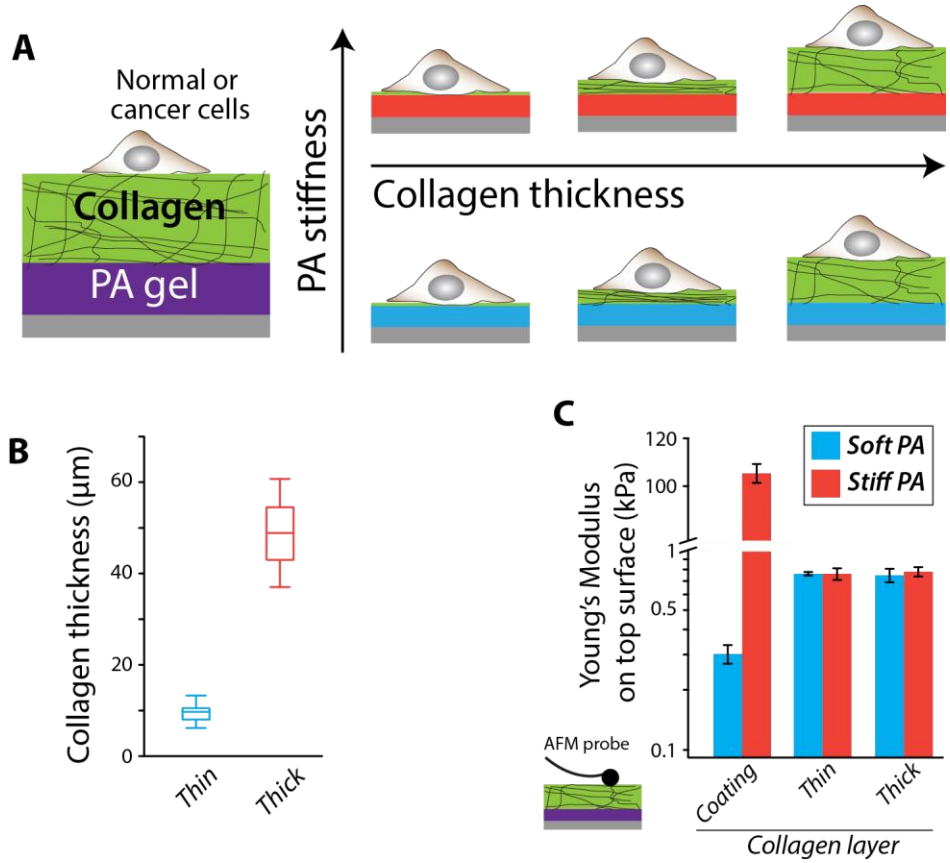

Figure 3.1. Fabrication and quantification of layered hydrogel substrates. (A) Representative diagram of all six layered hydrogel setups. **(B)** Quantification of collagen gel thickness of fabricated hydrogels. Box represents 10-90% of data with bar at mean value. Error Bars = SD. N>20. **(C)** Young's Moduli for all six layered hydrogel setups, as measured by AFM. Error Bars = SEM. N>30.

The normal epithelial cells (MCF-10A) migrated faster on stiffer PA gels with a monolayer coating of collagen. However, when seeded on either thin or thick collagen gels, they showed insignificant difference in migration speed or persistence (Figs. 3.2A,B) when compared against varying stiffness of the underlying PA stiffness. Normal cells did show a slight increase to the persistence of their migration, a measure of the overall displacement of a cell divided by its total distance traveled. Lower persistence values describe the so called 'wandering' cells that travel large distances while displacing a short distance from their origin, either by retracing their previous steps, or by seemingly "orbiting" around their origin point. Persistence values closer to 1 indicate cells with more directed migration, where every step they take contributes to increasing their overall displacement, much like a cancer cell breaking away from the tumor site. On thin collagen gels with stiff PA, normal cells showed 20% more persistent migration compared to coated gels, and their persistence continued to increase on thicker collagen gels, where they showed 30% more persistent migration (Fig. 3.2B). These results show that normal epithelial cells are unable to sense distant matrix stiffness and only respond to the properties of their immediate surroundings.

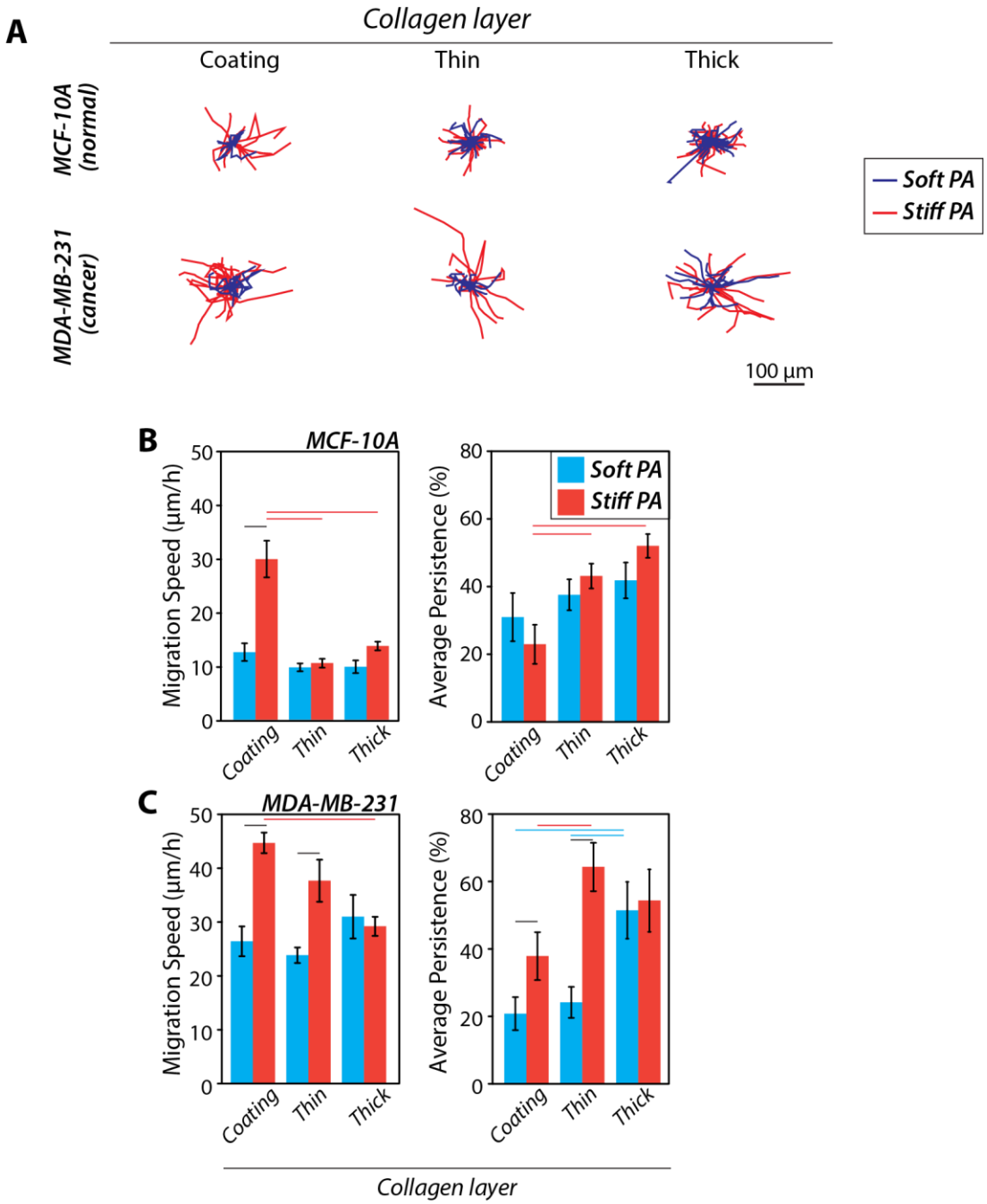

Figure 3.2. Cancerous epithelial cell migration is sensitive to distant stiffness on thin collagen platforms. (A) Representative cell migration trajectories for normal MCF10A and cancerous MDA-MB-231 epithelial cells. All tracks represent a 4 hr migration period with 30 min intervals. N = 15. Scale bar = 100 µm **(B & C)** Average cell migration and migratory persistence of **(B)** normal and **(C)** cancerous epithelial cells. Black horizontal bars represent significant statistical difference between values of the same collagen thickness, colored horizontal bars represent significant statistical difference between values of same PA stiffness. All $p < 0.01$. Error Bars = SEM. N>20.

In contrast, breast cancer cells (MDA-MB-231) showed a remarkable ability to distinguish distant stiffness on thin collagen gels. On both coating and thin collagen, cancer cells showed much faster migration with stiff PA, with an 80% increase on coating gels and a 40% increase on thin collagen gels. Interestingly, despite the similar migration speeds, cancer cells tended to "retrace" their own steps on stiff-coated gels, a behavior similar to cancer cells on soft gels and normal cells, yet they traveled large total distances (Fig. 3.2A). On stiff-thin substrates, cells covered large distances and displaced far away from their origin point, resulting in ~40% more persistent migration compared to stiff-coated substrates (Fig. 3.2C). As mentioned previously, cancer cells grown on soft-coated substrates had a tendency to retrace their steps, as seen by their short and compact trajectories (Fig. 3.2A). In contrast, cells on soft-thin and soft-thick substrates showed much more directed migration with 30% and 20% more persistent migration, respectively, compared to coated gels (Figs. 3.2A,C). On thick collagen gels, cancer cells were unable to sense distant stiffness, showing similar migration trajectories and equally persistent migration (Figs. 3.2A,C). The migration speeds on soft-thick versus stiff-thick matrices did not significantly differ, and were around the same magnitude as cells on soft-coated or soft-thin substrates (Fig. 3.2B). These findings indicate that a cancer cell's migration speed and trajectory is sensitive to both distant stiffness and its immediate surroundings, contrasting the response of normal epithelial cells.

3.3.2 Cancer cells exhibit elongated shapes and rise in stress fibers in response to distant layers of stiff matrix.

To further investigate the mechanism behind the cells' ability, or inability, to sense distant stiffness, we also analyzed the whole-body morphology and the intra-cellular actin structure of the cells on varying matrices. Both normal and cancer cells became more elongated on collagen gels thicker than a coating (Figs. 3.3A,B). Normal cells showed a significant increase in cell aspect ratio on thin or thick collagen gels, becoming ~50% more elongated, however they still remained much less elongated than cancer cells on the same substrates (Fig. 3.3B). Following this trend, normal cell roundness decreased on finite thickness collagen gels, showing ~50% reduction from soft-coated substrates and ~30% reduction compared to stiff-coated substrates (Fig. 3.3D). These changes to cell shape occurred with very little change to overall cell area, and normal cell areas were much smaller than those of cancer cells in general.

Similar to their migration behavior, cancer cells showed greater sensitivity to distant stiffness with their morphology. Cancer cells were nearly twice as elongated on thin and thick collagen substrates compared to coated substrates (Figs. 3.3A,B). Despite their high migration speeds, cancer cells were less elongated on stiff-coated substrates. Their area was also 50% larger than that of cells on any other substrate, and their roundness was twice that of cells on thin and thick collagen with stiff underlying PA (Figs. 3.3A-D).

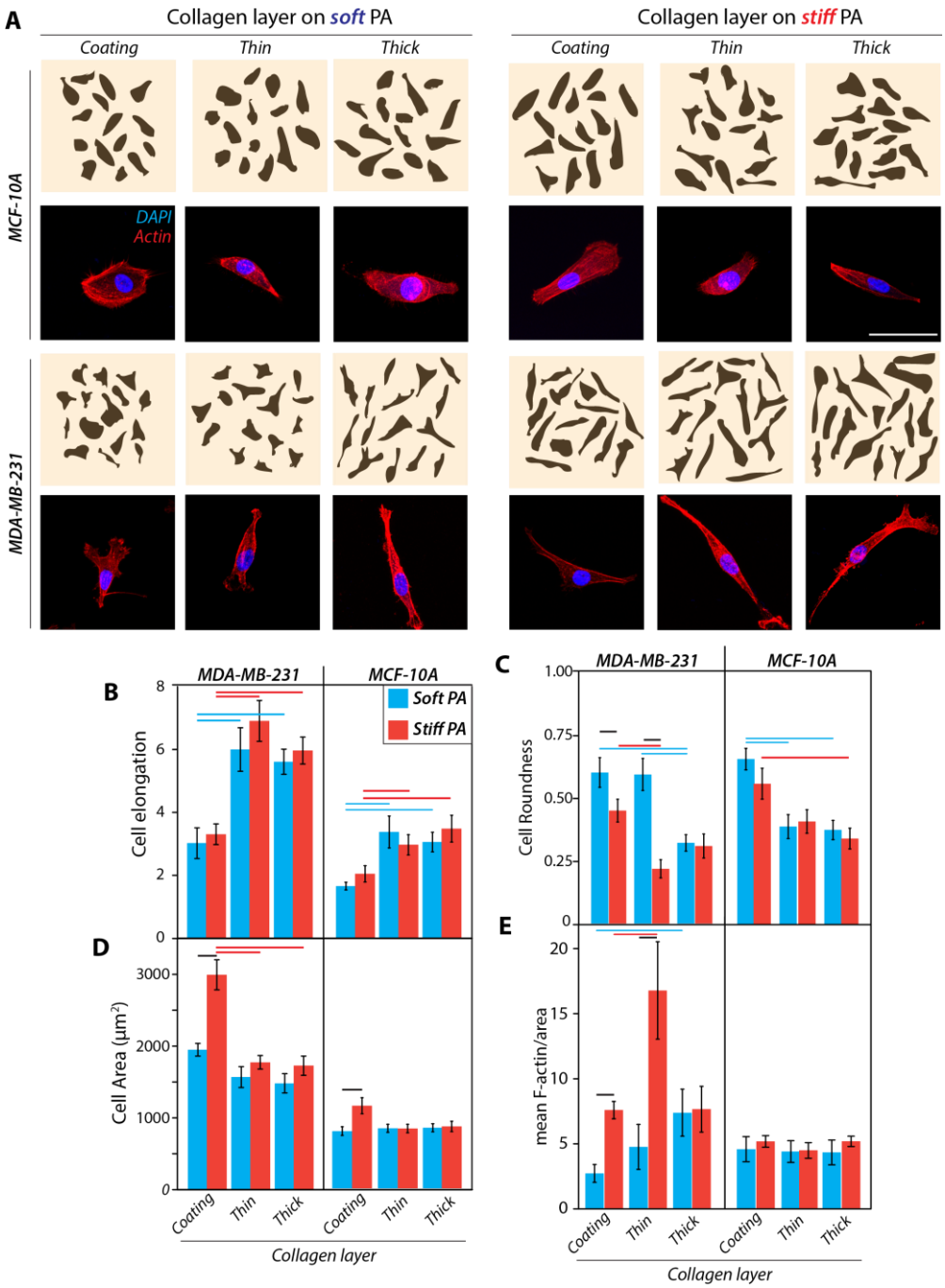
A
Collagen layer on soft PA
Collagen layer on stiff PA
Coating
Thin
Thick
MCF-10A
MDA-MB-231
DAPI
Actin
B
MDA-MB-231
MCF-10A
Soft PA
Stiff PA
Cell elongation
C
Cell Roundness
D
Cell Area (μm²)
E
mean F-actin/area
Collagen layer

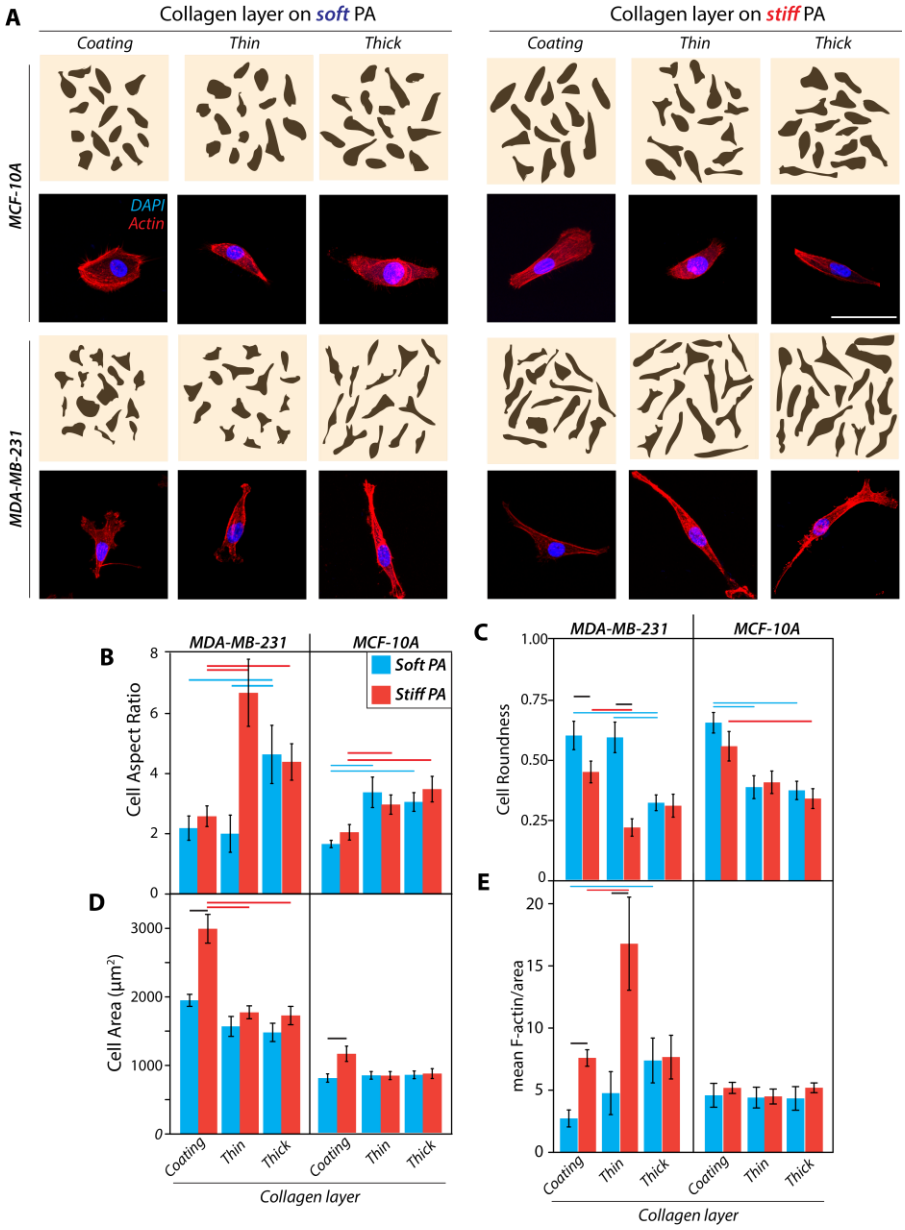

Figure 3.3. Cancerous epithelial cell morphology and actin cytoskeleton reflect distance sensitivity observed during cell migration. (A) Representative cell morphologies (top) and actin images (bottom) for normal MCF10A and cancerous MDA-MB-231 epithelial cells. N = 15 for representative morphologies. Scale bar = 50 μm **(B-E)** Average **(B)** cell aspect ratio, **(C)** roundness, **(D)**, spread area and **(E)** F-actin expression of normal and cancerous epithelial cells. Black horizontal bars represent significant statistical difference between values of the same collagen thickness, colored horizontal bars represent significant statistical difference between values of same PA stiffness. All $p < 0.01$. Error Bars = SEM. N>20.

This behavior on gels with collagen coating can be explained due to a lack of fibrous collagen

network to allow cells to optimally stretch and deform, thereby reducing their aspect ratio and increasing their roundness. Another notable phenomenon is that cancer cells on thin collagen gels with soft underlying PA were nearly three times rounder than cells on thick collagen or stiff underlying PA (Fig. 3.3D). Interestingly, these cells were still highly elongated. These cells appear to utilize the collagen architecture, resulting in high aspect ratio due to development of stable cell protrusions, to sense the distant soft PA, resulting in more rounded cell morphologies, similar to cells in immediate contact with soft PA (Figs. 3.2A,C).

Changes to cell morphology generally arise from modification to the internal cytoskeleton. To examine these intracellular changes, we stained and observed the actin fibers using phalloidin. The actin structure of normal cells did not significantly vary across any of the matrix conditions (Fig. 3.3E). By contrast, cancer cells showed large variations in actin structure, including a large increase in actin fiber accumulation on thin collagen substrates with stiff underlying PA. On both coating and thin collagen matrices, cancer cells showed ~3x the actin fiber accumulation with stiff underlying PA when compared to the soft PA layer. However, this difference in stiffness-sensitive actin structure disappeared on thick collagen gels. Cells on stiff-thin substrates also showed over twice as much actin fiber accumulation compared to cells on stiff-coated substrates. In case of a soft underlying PA layer, the actin fiber accumulation in cancer cells increased only when they sat atop a thick collagen gel.

3.3.3 Cancer cells sense distant matrix stiffness by deforming the intermediate collagen layer.

From the migration and morphology assays, cancer cells appear to be able to deform and align the surrounding collagen network to deform and sense the underlying PA gel. In order to

confirm this possibility and further investigate the extent of the depth sensing, we mixed beads into the collagen gel to track and measure the matrix deformation. In order to measure the deformation caused by cells, we first trypsinized the cells and then imaged bead positions over time to track their movements throughout the collagen layer. We then used the PIV lab tool in MATLAB to analyze the bead movements. In thin collagen gels, cancer cells were able to induce deformation throughout the entire collagen layer (Fig. 3.4A). Bead displacements within the collagen were most erratic on soft, thin gels, while bead movements in stiff-thin substrates and both soft-thick and stiff-thick platforms were fairly orderly (Fig. 3.4A). Notably, the magnitude of deformation was ~30 % higher on stiff-thin gels. We also measured small deformations within the top layer of the PA gel itself. On thin collagen gels, cell-generated deformations were able to reach the underlying PA, resulting in minor bead movements in the PA layer (Figs. 3.4A, B). On thick collagen, cells generated forces up to ~20 μm into the collagen. Since the matrix deformation did not transmit through the entire collagen layer, there was no deformation observed in the underlying PA layer (Fig. 3.4B).

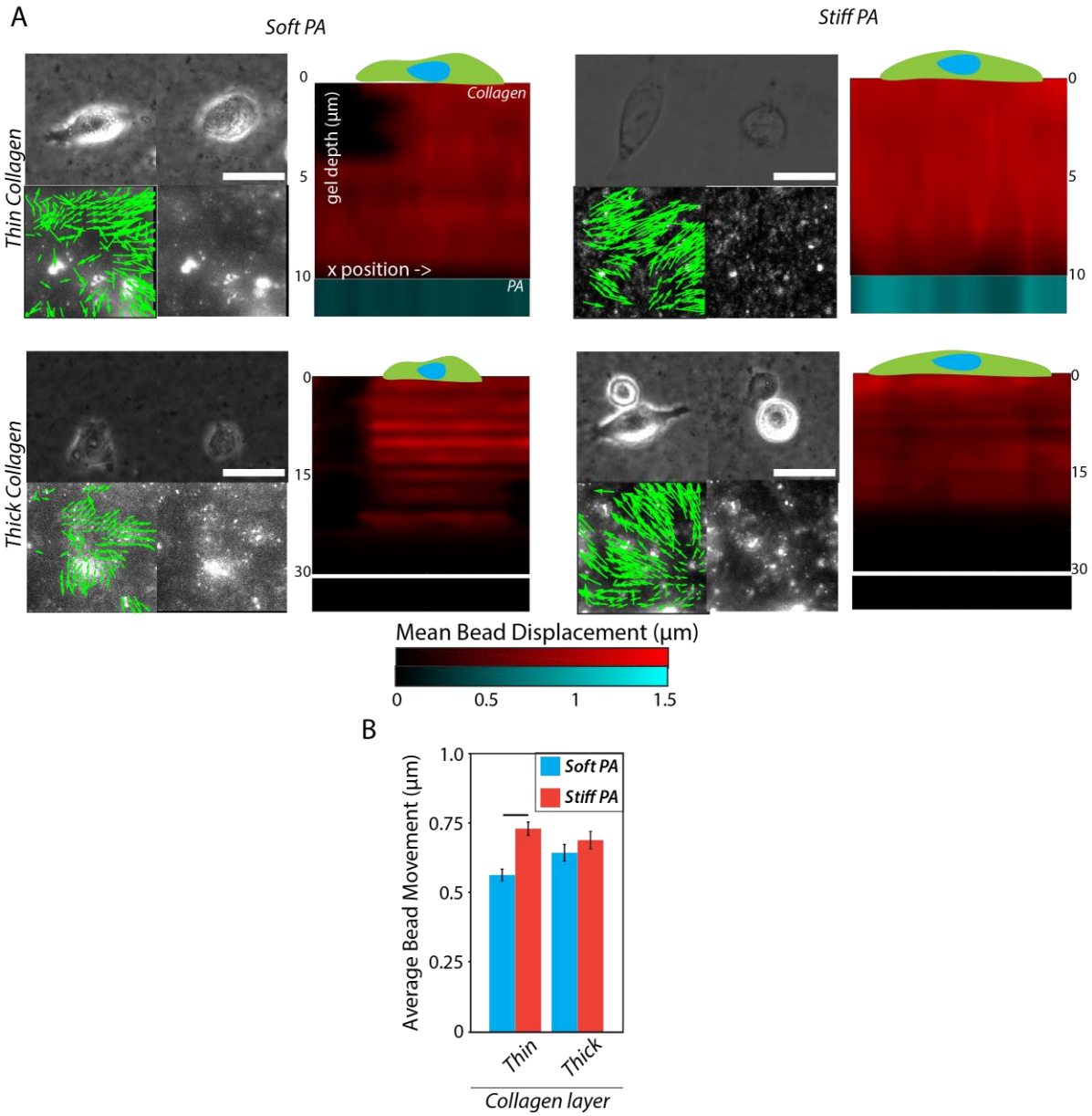

Figure 3.4. Cancerous epithelial cells sense distant PA stiffness through coordinated deformation of immediate collagen. (A, left) Representative images of cells and beads within collagen layer prior to (left) and after (right) release of cells. Scale bar = 25 μm **(A, right)** Representative bead displacement diagrams through the thickness of the collagen layer and at the collagen-PA interface. **(B)** Average bead displacement within collagen layer after release of the cell. Black horizontal bars represent significant statistical difference between values of the same collagen thickness. $p < 0.01$. Error Bars = SEM. N>5.

3.3.4 Loss of force generation disables depth-sensing in cancer cells.

To create the deformations seen in the collagen layer, cancer cells are likely to utilize both the fibrous and viscoelastic nature of the collagen matrix, as well as coordinated actin-myosin contractile networks. To confirm this behavior, we sought to restrict these two phenomena to understand their contribution to depth sensing. To eliminate coordinated cell contractile forces, we treated cells with Y27362 ROCK inhibitor, which inhibits the activation of ROCK by preventing the binding of RhoA, which activates ROCK 1/2 and promotes myosin contractility. When treated with ROCK inhibitor, cells had a tendency to produce uncoordinated protrusions (Fig. 3.5A). However, these protrusions did not lead to an increase in migration speed. On both thin and thick collagen gels, as well as soft and stiff PA, cell speed slowed compared to control cases (Fig. 3.5B). Cell migration was also far less persistent, resembling control cells on soft substrates (Fig. 3.5C). Despite their propensity to generate an increased number of protrusions, cells maintained mostly round bodies with very thin and random protrusions (Fig. 3.5A). This resulted in reductions in overall cell aspect ratio and total spread area, as well as an increase in cell roundness, compared to controls (Figs. 3.5A,D-F).

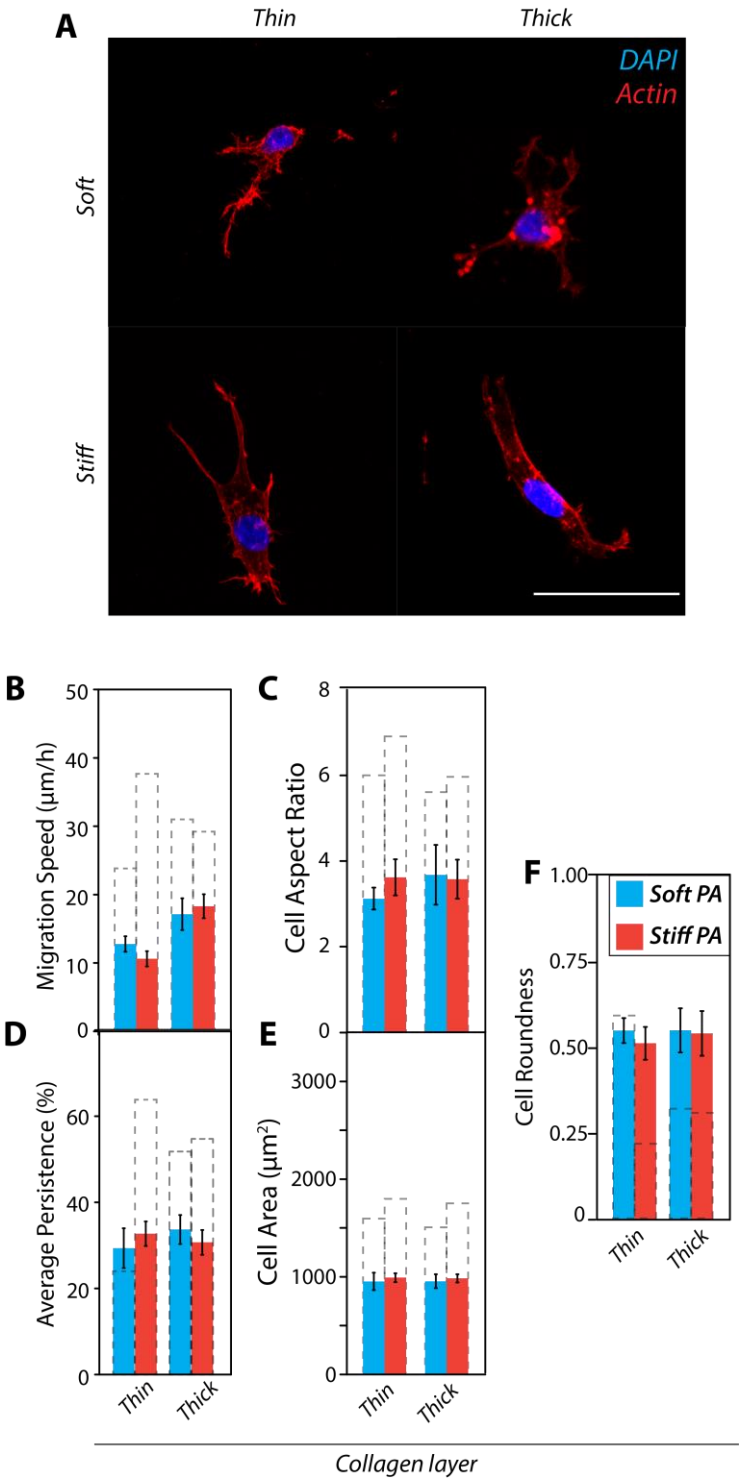

Figure 3.5. Loss of actin-myosin contractility inhibits cancer cell sensitivity to distant stiffness. (A) Representative actin images for MDA-MB-231 breast cancer cells after treatment with Y27362 ROCK inhibitor, with plots of average **(B)** migration speed, **(C)** cell aspect ratio, **(D)**, migratory persistence, **(E)** spread area, and **(F)** roundness. Scale bar = 50 μm. Grey dashed boxes represent values for untreated cells. Error Bars = SEM. N>20.

3.3.5 Crosslinking of the collagen layer disables cellular response to distant stiff matrix.

To externally disable the ability of cancer cells to deform the intermediate collagen layer without altering the intracellular machinery, we fabricated the layered gel setups and then treated the collagen with glutaraldehyde, a reagent that increases collagen crosslinking. By crosslinking the collagen prior to cell seeding, we reduce the viscous properties of the collagen substrate, creating a more linear elastic material, similar to the distant PA. This crosslinking is expected to restrict the cell's ability to deform the matrix. In contrast to cells treated with ROCK inhibitor, the untreated cells on layered substrates with cross-linked collagen showed increased migration speeds, similar to those on control stiff-thin substrates (Fig. 3.6B). Notably, the migration patterns of these cells showed very little persistence, similar to cells migrating on coated substrates (Fig. 3.6C). Similar to inhibition of ROCK, crosslinking of the collagen layer resulted in less elongated cells that were typically much smaller than cells on control collagen layers (Figs. 3.6D-F).

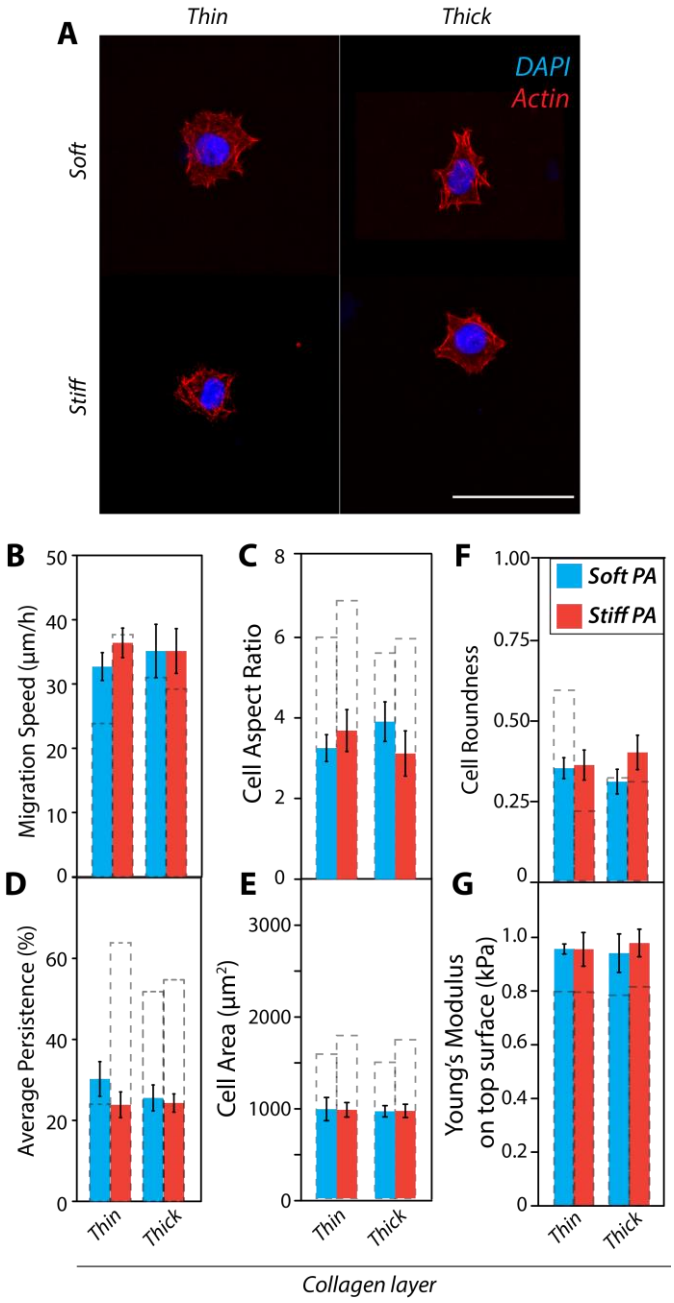

Figure 3.6. Crosslinking of fibrous collagen matrices inhibits cancer cell sensitivity to distant stiffness. (A) Representative actin images of MDA-MB-231 cells on layered substrates with thin or thick collagen layers, in which collagen was crosslinked by treatment with 0.05% glutaraldehyde. Scale bar = 50 μm. For the four matrix conditions of soft-thin, soft-thick, stiff-thin and stiff-thick, average **(B)** migration speed, **(C)** cell aspect ratio, **(D)**, migratory persistence, **(E)** spread area, and **(F)** roundness of cancerous epithelial cells cultured. Grey dashed boxes represent values for control (un-crosslinked) substrates. Error Bars = SEM. N>20. **(G)** Young's Moduli for layered hydrogel setups treated with 0.05% glutaraldehyde, as measured by AFM. Grey dashed boxes represent values for untreated substrates. Error Bars = SEM. N>20.

3.4 Discussion and Conclusions

We have shown that while normal epithelial cells show very little ability to sense distant stiffness, cancer cells were able to deform their immediate ECM to sense distant matrix properties. When cancer cells were cultured on thin collagen layers, their migration speed was much faster with stiff underlying PA. Cells cultured on finitely thick collagen layers also showed more persistent migration. When cultured on thick collagen gels, this stiffness-dependent difference diminished, and cells behaved the same with both soft and stiff underlying PA. As collagen thickness increased, cell aspect ratio followed suit, whereas cell area and cell roundness decreased. Interestingly, cancer cells on soft-thin substrates showed decreased cell aspect ratio and high cell roundness, behaving as though they were in direct contact of the underlying PA gels. Cancer cells were able to sense distant matrix stiffness through two mechanisms: adequate force generation through actin fiber assembly and myosin contractility, as well as the ability to deform their surrounding fibrous collagen matrix.

While this study is limited to only exploring the extent of distance sensing in 2D, observing how well these cells sense distant matrix properties in 3D is an important next step. Also, since we have found that the fibrous collagen network is crucial to a cell's ability to sense distant stiffness, we can next tune the properties of the fibers themselves, such as fiber size, to see what influence they have on distant stiffness sensing. We also do not control for matrix degradation or collagen bundling in this study, which could possibly be a critical mechanism utilized by cells to deform their immediate surrounding ECM to sense distant matrix properties.

Importantly, we found that the extent to which cancerous epithelial cells can sense distant matrix stiffness is in the range of 20 μm, much less than that seen from fibroblast cells, but much

greater than previously reported. There is a possibility that even normal epithelial cells could sense distant matrix properties to a greater extent than previously reported, although that limit is not explored here. This could implicate that the presence of a soft or stiff heterogeneity in the ECM, such as a tumor, could have an effect on more than just the cells in its immediate contact. This also could indicate that distant cells surrounding the tumor could also have an effect on the malignancy of that tumor.

Bibliography

1 Braga, V. M. M. & Yap, A. S. The challenges of abundance: epithelial junctions and small GTPase signalling. *Current Opinion in Cell Biology* **17**, 466-474, doi:https://doi.org/10.1016/j.ceb.2005.08.012 (2005).

2 Lodish, H. *et al. Molecular cell biology*. (Macmillan, 2008).

3 Shimoyama, Y. *et al.* Cadherin Cell-Adhesion Molecules in Human Epithelial Tissues and Carcinomas. *Cancer Research* **49**, 2128 (1989).

4 Qin, X. *et al.* Cell-matrix adhesion and cell-cell adhesion differentially control basal myosin oscillation and Drosophila egg chamber elongation. *Nature communications* **8**, 14708, doi:10.1038/ncomms14708 (2017).

5 Yurchenco, P. D. Basement membranes: cell scaffoldings and signaling platforms. *Cold Spring Harbor perspectives in biology* **3**, a004911, doi:10.1101/cshperspect.a004911 (2011).

6 Hagedorn, E. J. & Sherwood, D. R. Cell invasion through basement membrane: the anchor cell breaches the barrier. *Current Opinion in Cell Biology* **23**, 589-596, doi:https://doi.org/10.1016/j.ceb.2011.05.002 (2011).

7 Kalluri, R. Basement membranes: structure, assembly and role in tumour angiogenesis. *Nat Rev Cancer* **3**, 422-433, doi:10.1038/nrc1094 (2003).

8 Kelley, L. C., Lohmer, L. L., Hagedorn, E. J. & Sherwood, D. R. Traversing the basement membrane in vivo: A diversity of strategies. *The Journal of Cell Biology* **204**, 291 (2014).

9 Rowe, R. G. & Weiss, S. J. Navigating ECM Barriers at the Invasive Front: The Cancer Cell-Stroma Interface. *Annual Review of Cell and Developmental Biology* **25**, 567-595, doi:Doi 10.1146/Annurev.Cellbio.24.110707.175315 (2009).

10 Rowe, R. G. & Weiss, S. J. Breaching the basement membrane: who, when and how? *Trends Cell Biol* **18**, 560-574, doi:10.1016/j.tcb.2008.08.007 (2008).

11 Stuart, K., Paderi, J., Snyder, P. W., Freeman, L. & Panitch, A. Collagen-binding peptidoglycans inhibit MMP mediated collagen degradation and reduce dermal scarring. *PLoS One* **6**, e22139, doi:10.1371/journal.pone.0022139 (2011).

12 Jackson, D. & Cleary, E. The determination of collagen and elastin. *Methods Biochem Anal* **15**, 25-76 (1967).

13 Reiser, K., McCormick, R. J. & Rucker, R. B. Enzymatic and nonenzymatic cross-linking of collagen and elastin. *The FASEB Journal* **6**, 2439-2449, doi:10.1096/fasebj.6.7.1348714 (1992).

14 Kalluri, R. & Zeisberg, M. Fibroblasts in cancer. *Nature Reviews Cancer* **6**, 392-401, doi:10.1038/nrc1877 (2006).

15 Acton, S. E. *et al.* Dendritic cells control fibroblastic reticular network tension and lymph node expansion. *Nature* **514**, 498-502 (2014).

16 Heerboth, S. *et al.* EMT and tumor metastasis. *Clinical and Translational Medicine* **4**, 6, doi:10.1186/s40169-015-0048-3 (2015).

17 Ansieau, S. *et al.* Induction of EMT by Twist Proteins as a Collateral Effect of Tumor-Promoting Inactivation of Premature Senescence. *Cancer Cell* **14**, 79-89, doi:https://doi.org/10.1016/j.ccr.2008.06.005 (2008).
18 Huber, M. A., Kraut, N. & Beug, H. Molecular requirements for epithelial–mesenchymal transition during tumor progression. *Current Opinion in Cell Biology* **17**, 548-558, doi:https://doi.org/10.1016/j.ceb.2005.08.001 (2005).
19 Nasrollahi, S. & Pathak, A. Topographic confinement of epithelial clusters induces epithelial-to-mesenchymal transition in compliant matrices. *Scientific Reports* **6**, 18831, doi:10.1038/srep18831 (2016).
20 Kim, D. *et al.* DDR2 controls the epithelial-mesenchymal-transition-related gene expression via c-Myb acetylation upon matrix stiffening. *Sci Rep* **7**, 6847, doi:10.1038/s41598-017-07126-7 (2017).
21 Winer, J. P., Janmey, P. A., McCormick, M. E. & Funaki, M. Bone Marrow-Derived Human Mesenchymal Stem Cells Become Quiescent on Soft Substrates but Remain Responsive to Chemical or Mechanical Stimuli. *Tissue Engineering Part A* **15**, 147-154, doi:10.1089/ten.tea.2007.0388 (2008).
22 Engler, A. J., Sen, S., Sweeney, H. L. & Discher, D. E. Matrix elasticity directs stem cell lineage specification. *Cell* **126**, 677-689, doi:10.1016/j.cell.2006.06.044 (2006).
23 Lo, C.-M., Wang, H.-B., Dembo, M. & Wang, Y.-l. Cell Movement Is Guided by the Rigidity of the Substrate. *Biophysical Journal* **79**, 144-152, doi:http://dx.doi.org/10.1016/S0006-3495(00)76279-5 (2000).
24 Pathak, A. & Kumar, S. Transforming potential and matrix stiffness co-regulate confinement sensitivity of tumor cell migration. *Integr Biol (Camb)* **5**, 1067-1075, doi:10.1039/c3ib40017d
10.1039/c3ib40017d. (2013).
25 Wen, J. H. *et al.* Interplay of matrix stiffness and protein tethering in stem cell differentiation. *Nat Mater* **13**, 979-987, doi:10.1038/nmat4051
10.1038/nmat4051. Epub 2014 Aug 10. (2014).
26 Discher, D. E., Janmey, P. & Wang, Y.-l. Tissue Cells Feel and Respond to the Stiffness of Their Substrate. *Science* **310**, 1139-1143 (2005).
27 Kass, L., Erler, J. T., Dembo, M. & Weaver, V. M. Mammary epithelial cell: influence of extracellular matrix composition and organization during development and tumorigenesis. *Int J Biochem Cell Biol* **39**, 1987-1994, doi:10.1016/j.biocel.2007.06.025 (2007).
28 Rasmussen, C. H., Petersen, D. R., Moeller, J. B., Hansson, M. & Dufva, M. Collagen Type I Improves the Differentiation of Human Embryonic Stem Cells towards Definitive Endoderm. *PLoS One* **10**, e0145389, doi:10.1371/journal.pone.0145389
10.1371/journal.pone.0145389. eCollection 2015. (2015).
29 Das, S., Becker, B. N., Hoffmann, F. M. & Mertz, J. E. Complete reversal of epithelial to mesenchymal transition requires inhibition of both ZEB expression and the Rho pathway. *BMC cell biology* **10**, 94, doi:10.1186/1471-2121-10-94 (2009).
30 Lovisa, S. *et al.* Epithelial-to-mesenchymal transition induces cell cycle arrest and parenchymal damage in renal fibrosis. *Nat Med* **21**, 998-1009, doi:10.1038/nm.3902
http://www.nature.com/nm/journal/v21/n9/abs/nm.3902.html#supplementary-information (2015).

31 Yan, C. L. *et al.* Epithelial to Mesenchymal Transition in Human Skin Wound Healing Is Induced by Tumor Necrosis Factor-alpha through Bone Morphogenic Protein-2. *Am J Pathol* **176**, 2247-2258, doi:10.2353/ajpath.2010.090048 (2010).
32 Ahmadzadeh, H. *et al.* Modeling the two-way feedback between contractility and matrix realignment reveals a nonlinear mode of cancer cell invasion. *Proceedings of the National Academy of Sciences*, 201617037 (2017).
33 Arwert, E. N., Hoste, E. & Watt, F. M. Epithelial stem cells, wound healing and cancer. *Nature Reviews Cancer* **12**, 170-180, doi:10.1038/nrc3217 (2012).
34 Bajenaru, M. L. *et al.* Optic nerve glioma in mice requires astrocyte Nf1 gene inactivation and Nf1 brain heterozygosity. *Cancer Res* **63**, 8573-8577 (2003).
35 Baker, A. M., Bird, D., Lang, G., Cox, T. R. & Erler, J. T. Lysyl oxidase enzymatic function increases stiffness to drive colorectal cancer progression through FAK. *Oncogene* **32**, 1863-1868, doi:http://www.nature.com/onc/journal/v32/n14/suppinfo/onc2012202s1.html (2013).
36 Sporn, M. B. Approaches to Prevention of Epithelial Cancer during the Preneoplastic Period. *Cancer Research* **36**, 2699 (1976).
37 Voulgari, A. & Pintzas, A. Epithelial–mesenchymal transition in cancer metastasis: Mechanisms, markers and strategies to overcome drug resistance in the clinic. *Biochimica et Biophysica Acta (BBA) - Reviews on Cancer* **1796**, 75-90, doi:https://doi.org/10.1016/j.bbcan.2009.03.002 (2009).
38 Levayer, R. & Lecuit, T. Breaking down EMT. *Nature Cell Biology* **10**, 757, doi:10.1038/ncb0708-757 (2008).
39 NCI. *Metastatic Cancer*, <https://www.cancer.gov/types/metastatic-cancer#where-cancer-spreads> (2017).
40 Huang, H. *et al.* Up-regulation of N-cadherin by Collagen I-activated Discoidin Domain Receptor 1 in Pancreatic Cancer Requires the Adaptor Molecule Shc1. *The Journal of biological chemistry* **291**, 23208-23223, doi:10.1074/jbc.M116.740605 (2016).
41 Jung, H.-Y. *et al.* Apical–basal polarity inhibits epithelial–mesenchymal transition and tumour metastasis by PAR-complex-mediated SNAI1 degradation. *Nature Cell Biology* **21**, 359-371, doi:10.1038/s41556-019-0291-8 (2019).
42 Nakaya, Y., Sukowati, E. W., Wu, Y. & Sheng, G. J. RhoA and microtubule dynamics control cell-basement membrane interaction in EMT during gastrulation. *Nature Cell Biology* **10**, 765-775, doi:10.1038/ncb1739 (2008).
43 Ivaska, J. Vimentin. *Small GTPases* **2**, 51-53, doi:10.4161/sgtp.2.1.15114 (2011).
44 Wang, Y. *et al.* Akt/Ezrin Tyr353/NF-kappaB pathway regulates EGF-induced EMT and metastasis in tongue squamous cell carcinoma. *British journal of cancer* **110**, 695-705, doi:10.1038/bjc.2013.770 (2014).
45 Scarpa, E. & Mayor, R. Collective cell migration in development. *The Journal of Cell Biology* **212**, 143, doi:10.1083/jcb.201508047 (2016).
46 Li, L., He, Y., Zhao, M. & Jiang, J. Collective cell migration: Implications for wound healing and cancer invasion. *Burns Trauma* **1**, 21-26, doi:10.4103/2321-3868.113331 (2013).

47 Lauffenburger, D. A. & Horwitz, A. F. Cell Migration: A Physically Integrated Molecular Process. *Cell* **84**, 359-369, doi:http://dx.doi.org/10.1016/S0092-8674(00)81280-5 (1996).
48 Plant, A. L., Bhadriraju, K., Spurlin, T. A. & Elliott, J. T. Cell response to matrix mechanics: focus on collagen. *Biochim Biophys Acta* **1793**, 893-902, doi:10.1016/j.bbamcr.2008.10.012
10.1016/j.bbamcr.2008.10.012. Epub 2008 Nov 5. (2009).
49 Yam, P. T. *et al.* Actin-myosin network reorganization breaks symmetry at the cell rear to spontaneously initiate polarized cell motility. *J Cell Biol* **178**, 1207-1221, doi:10.1083/jcb.200706012 (2007).
50 Engler, A. *et al.* Substrate Compliance versus Ligand Density in Cell on Gel Responses. *Biophysical Journal* **86**, 617-628 (2004).
51 Nomura, H., Naito, M., Iguchi, A., Douglas Thompson, W. & Smith, E. B. Fibrin Gel Induces the Migration of Smooth Muscle Cells from Rabbit Aortic Explants. *Thrombosis and Haemostasis* **82**, 1347-1352 (1999).
52 Peyton, S. R., Kim, P. D., Ghajar, C. M., Seliktar, D. & Putnam, A. J. The effects of matrix stiffness and RhoA on the phenotypic plasticity of smooth muscle cells in a 3-D biosynthetic hydrogel system. *Biomaterials* **29**, 2597-2607, doi:10.1016/j.biomaterials.2008.02.005
10.1016/j.biomaterials.2008.02.005. Epub 2008 Mar 14. (2008).
53 Peyton, S. R. & Putnam, A. J. Extracellular matrix rigidity governs smooth muscle cell motility in a biphasic fashion. *Journal of Cellular Physiology* **204**, 198-209, doi:10.1002/jcp.20274 (2005).
54 Nasrollahi, S., Banerjee, S., Qayum, B., Banerjee, P. & Pathak, A. Nano-scale matrix topography influences micro-scale cell motility through adhesions, actin organization, and cell shape. *ACS Biomaterials Science & Engineering*, doi:10.1021/acsbiomaterials.6b00554 (2016).
55 Pathak, A. & Kumar, S. Independent regulation of tumor cell migration by matrix stiffness and confinement. *Proceedings of the National Academy of Sciences* **109**, 10334-10339, doi:papers2://publication/doi/10.1073/pnas.1118073109 (2012).
56 Zhang, K. *et al.* Mechanical signals regulate and activate SNAIL1 protein to control the fibrogenic response of cancer-associated fibroblasts. *Journal of Cell Science* **129**, 1989, doi:10.1242/jcs.180539 (2016).
57 Koh, M. *et al.* Discoidin domain receptor 1 is a novel transcriptional target of ZEB1 in breast epithelial cells undergoing H-Ras-induced epithelial to mesenchymal transition. *International journal of cancer* **136**, E508-E520 (2015).
58 Sunyer, R. *et al.* Collective cell durotaxis emerges from long-range intercellular force transmission. *Science* **353**, 1157-1161 (2016).
59 Lee, J., Abdeen, A. A., Wycislo, K. L., Fan, T. M. & Kilian, K. A. Interfacial geometry dictates cancer cell tumorigenicity. *Nat Mater*, doi:10.1038/nmat4610
10.1038/nmat4610. (2016).
60 Buxboim, A., Ivanovska, I. L. & Discher, D. E. Matrix elasticity, cytoskeletal forces and physics of the nucleus: how deeply do cells 'feel' outside and in? *J Cell Sci* **123**, 297-308, doi:10.1242/jcs.041186
10.1242/jcs.041186. (2010).

61 Maloney, J. M., Walton, E. B., Bruce, C. M. & Van Vliet, K. J. Influence of finite thickness and stiffness on cellular adhesion-induced deformation of compliant substrata. *Phys Rev E Stat Nonlin Soft Matter Phys* **78**, 041923, doi:10.1103/PhysRevE.78.041923 (2008).
62 Engler, A. J., Richert, L., Wong, J. Y., Picart, C. & Discher, D. E. Surface probe measurements of the elasticity of sectioned tissue, thin gels and polyelectrolyte multilayer films: Correlations between substrate stiffness and cell adhesion. *Surface Science* **570**, 142-154, doi:10.1016/j.susc.2004.06.179 (2004).
63 Fischer, R. S., Myers, K. A., Gardel, M. L. & Waterman, C. M. Stiffness-controlled three-dimensional extracellular matrices for high-resolution imaging of cell behavior. *Nat Protoc* **7**, 2056-2066, doi:10.1038/nprot.2012.127
10.1038/nprot.2012.127. Epub 2012 Oct 25. (2012).
64 Fraley, S. I. *et al.* Three-dimensional matrix fiber alignment modulates cell migration and MT1-MMP utility by spatially and temporally directing protrusions. *Sci Rep* **5**, 14580, doi:10.1038/srep14580
10.1038/srep14580. (2015).
65 Ulrich, T. A., de Juan Pardo, E. M. & Kumar, S. The mechanical rigidity of the extracellular matrix regulates the structure, motility, and proliferation of glioma cells. *Cancer Res* **69**, 4167-4174, doi:10.1158/0008-5472.CAN-08-4859
10.1158/0008-5472.CAN-08-4859. Epub 2009 May 12. (2009).
66 Ulrich, T. A., Jain, A., Tanner, K., MacKay, J. L. & Kumar, S. Probing cellular mechanobiology in three-dimensional culture with collagen-agarose matrices. *Biomaterials* **31**, 1875-1884, doi:10.1016/j.biomaterials.2009.10.047
10.1016/j.biomaterials.2009.10.047. Epub 2009 Nov 18. (2010).
67 Nistico, P., Bissell, M. J. & Radisky, D. C. Epithelial-mesenchymal transition: general principles and pathological relevance with special emphasis on the role of matrix metalloproteinases. *Cold Spring Harbor perspectives in biology* **4**, doi:10.1101/cshperspect.a011908 (2012).
68 Sherwood, D. R. Cell invasion through basement membranes: an anchor of understanding. *Trends Cell Biol.* **16**, 250-256, doi:10.1016/j.tcb.2006.03.004 (2006).
69 Yurchenco, P. D. Basement membranes: cell scaffoldings and signaling platforms. *Cold Spring Harbor perspectives in biology* **3**, doi:10.1101/cshperspect.a004911 (2011).
70 Carraro, D. M., Elias, E. V. & Andrade, V. P. Ductal carcinoma in situ of the breast: morphological and molecular features implicated in progression. *Biosci Rep* **34**, doi:10.1042/BSR20130077 (2014).
71 Kalluri, R. Discovery of Type IV Collagen Non-collagenous Domains as Novel Integrin Ligands and Endogenous Inhibitors of Angiogenesis. *Cold Spring Harbor Symposia on Quantitative Biology* **67**, 255-266 (2002).
72 Timpl, R., Wiedemann, H., Van Delden, V., Furthmayr, H. & KÜHn, K. A Network Model for the Organization of Type IV Collagen Molecules in Basement Membranes. *European Journal of Biochemistry* **120**, 203-211, doi:10.1111/j.1432-1033.1981.tb05690.x (1981).
73 Leight, J. L., Wozniak, M. A., Chen, S., Lynch, M. L. & Chen, C. S. Matrix rigidity regulates a switch between TGF-beta1-induced apoptosis and epithelial-

mesenchymal transition. *Molecular biology of the cell* **23**, 781-791, doi:10.1091/mbc.E11-06-0537 (2012).
74 Lee, K. *et al.* Matrix compliance regulates Rac1b localization, NADPH oxidase assembly, and epithelial-mesenchymal transition. *Molecular biology of the cell* **23**, 4097-4108, doi:10.1091/mbc.E12-02-0166 (2012).
75 Wei, S. C. *et al.* Matrix stiffness drives epithelial-mesenchymal transition and tumour metastasis through a TWIST1-G3BP2 mechanotransduction pathway. *Nat Cell Biol*, doi:10.1038/ncb3157 (2015).
76 Pathak, A. Scattering of Cell Clusters in Confinement. *Biophysical journal* **111**, 1496-1506, doi:10.1016/j.bpj.2016.08.034 (2016).
77 Gomez Esther, W., Chen Qike, K., Gjorevski, N. & Nelson Celeste, M. Tissue geometry patterns epithelial–mesenchymal transition via intercellular mechanotransduction. *Journal of Cellular Biochemistry* **110**, 44-51, doi:10.1002/jcb.22545 (2010).
78 Brown, A. C., Fiore, V. F., Sulchek, T. A. & Barker, T. H. Physical and chemical microenvironmental cues orthogonally control the degree and duration of fibrosis-associated epithelial-to-mesenchymal transitions. *The Journal of pathology* **229**, 25-35, doi:10.1002/path.4114 (2013).
79 Van Hoof, J. & Harrisson, F. Interaction between epithelial basement membrane and migrating mesoblast cells in the avian blastoderm. *Differentiation* **32**, 120-124 (1986).
80 Petersen, O. W., Ronnov-Jessen, L., Howlett, A. R. & Bissell, M. J. Interaction with basement membrane serves to rapidly distinguish growth and differentiation pattern of normal and malignant human breast epithelial cells. *Proc Natl Acad Sci U S A* **89**, 9064-9068 (1992).
81 Esposito, N. N., Dabbs, D. J. & Bhargava, R. Are encapsulated papillary carcinomas of the breast in situ or invasive? A basement membrane study of 27 cases. *Am J Clin Pathol* **131**, 228-242, doi:10.1309/AJCP8A2UVLCYGTPU (2009).
82 Nasrollahi, S. *et al.* Past matrix stiffness primes epithelial cells and regulates their future collective migration through a mechanical memory. *Biomaterials* **146**, 146-155, doi:10.1016/j.biomaterials.2017.09.012 (2017).
83 Pathak, A. & Kumar, S. Transforming potential and matrix stiffness co-regulate confinement sensitivity of tumor cell migration. *Integr. Biol.* **5**, 1067-1075, doi:10.1039/c3ib40017d (2013).
84 Debnath, J., Muthuswamy, S. K. & Brugge, J. S. Morphogenesis and oncogenesis of MCF-10A mammary epithelial acini grown in three-dimensional basement membrane cultures. *Methods* **30**, 256-268, doi:http://dx.doi.org/10.1016/S1046-2023(03)00032-X (2003).
85 Livak, K. J. & Schmittgen, T. D. Analysis of Relative Gene Expression Data Using Real-Time Quantitative PCR and the 2−ΔΔCT Method. *Methods* **25**, 402-408, doi:https://doi.org/10.1006/meth.2001.1262 (2001).
86 Walter, C. *et al.* Increased Tissue Stiffness in Tumors from Mice with Neurofibromatosis-1 Optic Glioma. *Biophysical journal* **112**, 1535-1538, doi:http://doi.org/10.1016/j.bpj.2017.03.017 (2017).

87 Chalhoub, N. & Baker, S. J. PTEN and the PI3-kinase pathway in cancer. *Annual review of pathology* **4**, 127-150, doi:10.1146/annurev.pathol.4.110807.092311 (2009).
88 Ren, Y. *et al.* PTEN activation sensitizes breast cancer to PI3-kinase inhibitor through the beta-catenin signaling pathway. *Oncology reports* **28**, 943-948, doi:10.3892/or.2012.1856 (2012).
89 Zeng, Z. S., Cohen, A. M. & Guillem, J. G. Loss of basement membrane type IV collagen is associated with increased expression of metalloproteinases 2 and 9 (MMP-2 and MMP-9) during human colorectal tumorigenesis. *Carcinogenesis* **20**, 749-755 (1999).
90 Paszek, M. J. *et al.* Tensional homeostasis and the malignant phenotype. *Cancer Cell* **8**, 241-254 (2005).
91 Ulrich, T. A., de Juan Pardo, E. M. & Kumar, S. The mechanical rigidity of the extracellular matrix regulates the structure, motility, and proliferation of glioma cells. *Cancer Res.* **69**, 4167-4174, doi:papers2://publication/doi/10.1158/0008-5472.CAN-08-4859 (2009).
92 Sabeh, F., Shimizu-Hirota, R. & Weiss, S. J. Protease-dependent versus -independent cancer cell invasion programs: three-dimensional amoeboid movement revisited. *The Journal of Cell Biology* **185**, 11-19, doi:10.1083/jcb.200807195 (2009).
93 Beadle, C. *et al.* The Role of Myosin II in Glioma Invasion of the Brain. *Molecular biology of the cell* **19**, 3357-3368, doi:10.1091/mbc.E08-03-0319 (2008).
94 Kun Zhang *et al.* Mechanical signals regulate and activate SNAIL1 protein to control the fibrogenic response of cancer-associated fibroblasts. *Journal of Cell Science* **(in press)**, doi:10.1242/jcs.180539, doi:doi:10.1242/jcs.180539 (2016).
95 McKnight, A. L. *et al.* MR Elastography of Breast Cancer: Preliminary Results. *American Journal of Roentgenology* **178**, 1411-1417, doi:10.2214/ajr.178.6.1781411 (2002).
96 Miyaji, K. *et al.* The stiffness of lymph nodes containing lung carcinoma metastases. *Cancer* **80**, 1920-1925, doi:10.1002/(SICI)1097-0142(19971115)80:10<1920::AID-CNCR8>3.0.CO;2-R (1997).
97 Kallioinen, M., Autio-Harmainen, H., Dammert, K., Risteli, J. & Risteli, L. Discontinuity of the Basement Membrane in Fibrosing Basocellular Carcinomas and Basosquamous Carcinomas of the Skin: An Immunohistochemical Study with Human Laminin and Type IV Collagen Antibodies. *Journal of Investigative Dermatology* **82**, 248-251, doi:http://dx.doi.org/10.1111/1523-1747.ep12260190 (1984).
98 Kallioinen, M., Autio-Harmainen, H., Dammert, K., Risteli, J. & Risteli, L. Discontinuity of the basement membrane in fibrosing basocellular carcinomas and basosquamous carcinomas of the skin: an immunohistochemical study with human laminin and type IV collagen antibodies. *J Invest Dermatol* **82**, 248-251 (1984).
99 Espinosa Neira, R. & Salazar, E. P. Native type IV collagen induces an epithelial to mesenchymal transition-like process in mammary epithelial cells MCF10A. *The International Journal of Biochemistry & Cell Biology* **44**, 2194-2203, doi:https://doi.org/10.1016/j.biocel.2012.08.018 (2012).

100 Radisky, E. S. & Radisky, D. C. Matrix metalloproteinase-induced epithelial-mesenchymal transition in breast cancer. *Journal of mammary gland biology and neoplasia* **15**, 201-212, doi:10.1007/s10911-010-9177-x (2010).
101 Lin, C. Y. *et al.* Matrix metalloproteinase-9 cooperates with transcription factor Snail to induce epithelial-mesenchymal transition. *Cancer science* **102**, 815-827, doi:10.1111/j.1349-7006.2011.01861.x (2011).
102 Tan, T. K. *et al.* Macrophage matrix metalloproteinase-9 mediates epithelial-mesenchymal transition in vitro in murine renal tubular cells. *Am J Pathol* **176**, 1256-1270, doi:10.2353/ajpath.2010.090188 (2010).
103 Hiratsuka, S. *et al.* MMP9 induction by vascular endothelial growth factor receptor-1 is involved in lung-specific metastasis. *Cancer Cell* **2**, 289-300, doi:https://doi.org/10.1016/S1535-6108(02)00153-8 (2002).
104 Mehner, C. *et al.* Tumor cell-produced matrix metalloproteinase 9 (MMP-9) drives malignant progression and metastasis of basal-like triple negative breast cancer. *Oncotarget* **5**, 2736-2749, doi:10.18632/oncotarget.1932 (2014).
105 Mendes, O., Kim, H.-T. & Stoica, G. Expression of MMP2, MMP9 and MMP3 in Breast Cancer Brain Metastasis in a Rat Model. *Clinical & experimental metastasis* **22**, 237-246, doi:10.1007/s10585-005-8115-6 (2005).
106 Wolf, K. *et al.* Physical limits of cell migration: Control by ECM space and nuclear deformation and tuning by proteolysis and traction force. *The Journal of Cell Biology* **201**, 1069-1084, doi:papers2://publication/doi/10.1073/pnas.0604460103 (2013).
107 Ota, I., Li, X.-Y., Hu, Y. & Weiss, S. J. Induction of a MT1-MMP and MT2-MMP-dependent basement membrane transmigration program in cancer cells by Snail1. *Proc. Natl. Acad. Sci. U.S.A.* **106**, 20318 (2009).
108 Chaudhuri, O. *et al.* Extracellular matrix stiffness and composition jointly regulate the induction of malignant phenotypes in mammary epithelium. *Nature materials* **13**, 970-978, doi:10.1038/nmat4009 (2014).
109 Benton, G., Crooke, E. & George, J. Laminin-1 induces E-cadherin expression in 3-dimensional cultured breast cancer cells by inhibiting DNA methyltransferase 1 and reversing promoter methylation status. *The FASEB Journal* **23**, 3884-3895, doi:10.1096/fj.08-128702 (2009).
110 Wullkopf, L. *et al.* Cancer cells' ability to mechanically adjust to extracellular matrix stiffness correlates with their invasive potential. *Molecular Biology of the Cell* **29**, 2378-2385, doi:10.1091/mbc.E18-05-0319 (2018).
111 Schedin, P. & Keely, P. J. Mammary gland ECM remodeling, stiffness, and mechanosignaling in normal development and tumor progression. *Cold Spring Harb Perspect Biol* **3**, a003228, doi:10.1101/cshperspect.a003228
10.1101/cshperspect.a003228. (2011).
112 Wisdom, K. M. *et al.* Matrix mechanical plasticity regulates cancer cell migration through confining microenvironments. *Nature communications* **9**, 4144, doi:10.1038/s41467-018-06641-z (2018).
113 Califano, J. P. & Reinhart-King, C. A. Substrate Stiffness and Cell Area Predict Cellular Traction Stresses in Single Cells and Cells in Contact. *Cell Mol Bioeng* **3**, 68-75, doi:10.1007/s12195-010-0102-6 (2010).

114 Riching, K. M. *et al.* 3D collagen alignment limits protrusions to enhance breast cancer cell persistence. *Biophys J* **107**, 2546-2558, doi:10.1016/j.bpj.2014.10.035 10.1016/j.bpj.2014.10.035. Epub 2014 Dec 2. (2014).
115 Aubin, H. *et al.* Directed 3D cell alignment and elongation in microengineered hydrogels. *Biomaterials* **31**, 6941-6951, doi:http://dx.doi.org/10.1016/j.biomaterials.2010.05.056 (2010).
116 Guzman, A., Ziperstein, M. J. & Kaufman, L. J. The effect of fibrillar matrix architecture on tumor cell invasion of physically challenging environments. *Biomaterials* **35**, 6954-6963, doi:10.1016/j.biomaterials.2014.04.086 10.1016/j.biomaterials.2014.04.086. Epub 2014 May 15. (2014).
117 Provenzano, P. P., Eliceiri, K. W., Inman, D. R. & Keely, P. J. Engineering Three-Dimensional Collagen Matrices to Provide Contact Guidance during 3D Cell Migration. *Current Protocols in Cell Biology*, 10.17. 11-10.17. 11 (2010).
118 Wolf, K. *et al.* Physical limits of cell migration: control by ECM space and nuclear deformation and tuning by proteolysis and traction force. *J Cell Biol* **201**, 1069-1084 (2013).
119 Haugh, M. G., Murphy, C. M., McKiernan, R. C., Altenbuchner, C. & O'Brien, F. J. Crosslinking and Mechanical Properties Significantly Influence Cell Attachment, Proliferation, and Migration Within Collagen Glycosaminoglycan Scaffolds. *Tissue Engineering Part A* **17**, 1201-1208, doi:10.1089/ten.tea.2010.0590 (2010).
120 Wolf, K. *et al.* Compensation mechanism in tumor cell migration. *mesenchymal–amoeboid transition after blocking of pericellular proteolysis* **160**, 267-277, doi:10.1083/jcb.200209006 (2003).
121 Sabeh, F. *et al.* Tumor cell traffic through the extracellular matrix is controlled by the membrane-anchored collagenase MT1-MMP. *The Journal of Cell Biology* **167**, 769, doi:10.1083/jcb.200408028 (2004).
122 Acerbi, I. *et al.* Human breast cancer invasion and aggression correlates with ECM stiffening and immune cell infiltration. *Integrative Biology* **7**, 1120-1134, doi:10.1039/c5ib00040h (2015).
123 Georges, P. C. *et al.* Increased stiffness of the rat liver precedes matrix deposition: implications for fibrosis. *American Journal of Physiology-Gastrointestinal and Liver Physiology* **293**, G1147-G1154, doi:10.1152/ajpgi.00032.2007 (2007).
124 Conrad, C. H. *et al.* Myocardial Fibrosis and Stiffness With Hypertrophy and Heart Failure in the Spontaneously Hypertensive Rat. *Circulation* **91**, 161-170, doi:doi:10.1161/01.CIR.91.1.161 (1995).
125 Marcellin, P. *et al.* Non-invasive assessment of liver fibrosis by stiffness measurement in patients with chronic hepatitis B. *Liver International* **29**, 242-247, doi:10.1111/j.1478-3231.2008.01802.x (2009).
126 Munevar, S., Wang, Y.-l. & Dembo, M. Traction Force Microscopy of Migrating Normal and H-ras Transformed 3T3 Fibroblasts. *Biophysical Journal* **80**, 1744-1757, doi:http://dx.doi.org/10.1016/S0006-3495(01)76145-0 (2001).
127 Sunyer, R. *et al.* Collective cell durotaxis emerges from long-range intercellular force transmission. *Science* **353**, 1157 (2016).
128 Serra-Picamal, X., Conte, V., Sunyer, R., Muñoz, J. J. & Trepat, X. in *Methods in Cell Biology* Vol. 125 (ed Ewa K. Paluch) 309-330 (Academic Press, 2015).

129 Pakshir, P. *et al.* Dynamic fibroblast contractions attract remote macrophages in fibrillar collagen matrix. *Nature communications* **10**, 1850, doi:10.1038/s41467-019-09709-6 (2019).
130 Schnitt, S. J., Silen, W., Sadowsky, N. L., Connolly, J. L. & Harris, J. R. Ductal carcinoma in situ (intraductal carcinoma) of the breast. *New England Journal of Medicine* **318**, 898-903 (1988).
131 Hu, M. & Polyak, K. Microenvironmental regulation of cancer development. *Current Opinion in Genetics & Development* **18**, 27-34, doi:https://doi.org/10.1016/j.gde.2007.12.006 (2008).
132 William, T. & Eize, J. S. *PIVlab - Time-Resolved Digital Particle Image Velocimetry Tool for MATLAB*. (2019).
133 Thielicke, W. & Stamhuis, E. PIVlab–towards user-friendly, affordable and accurate digital particle image velocimetry in MATLAB. *Journal of Open Research Software* **2** (2014).